Arabian Journal of Chemistry (2023) **16**, 104643

King Saud University

Arabian Journal of Chemistry

www.ksu.edu.sa
www.sciencedirect.com

ORIGINAL ARTICLE

Insight the mechanism of MgAl/layered double hydroxide supported on rubber seed shell biochar for Remazol Brilliant Violet 5R removal

Shahreen Izwan Anthonysamy [a], **Mohd Azmier Ahmad** [a,*], **Nasehir Khan E.M. Yahaya** [b]

[a] *School of Chemical Engineering, Engineering Campus, Universiti Sains Malaysia, 14300 Nibong Tebal, Seberang Perai Selatan, Pulau Pinang, Malaysia*
[b] *National Water Research Institute of Malaysia (NAHRIM), Ministry of Natural Resources, Environment and Climate Change, Lot 5377, Jalan Putra Permai, 43300 Seri Kembangan, Selangor, Malaysia*

Received 23 September 2022; accepted 29 January 2023
Available online 1 February 2023

KEYWORDS

Biochar;
Remazol Brilliant Violet 5R;
Rubber seed shell;
Endothermic;
Physisorption

Abstract The ever-increasing concentration of Remazol Brilliant Violet 5R discharged mainly from textile industry had cause serious environmental issues towards human and the surrounding ecosystem. Therefore, solving the issue related to dye contamination is seriously important. In this research study, MgAl/layered double hydroxide supported on rubber seed shell biochar (RSSB) had been prepared for Remazol Brilliant Violet 5R (RBV5R) dye adsorption. BET surface area and pore volume of RSSB were found to be 132.40 m^2/g and 0.0732 cm^3/g, respectively with presence of LDH metals on the RSSB surfaces. The batch adsorption studies showed that RBV5R uptake capacity was significantly enhanced (125.88 mg/g) compared to pristine RSSB (58.69 mg/g) at initial RBV5R concentration, contact time, adsorption temperature and pH of 300 mg/l, 1440 min, 60 °C and pH 2, respectively. The equilibrium and kinetic adsorption data were best fitted into the Freundlich and pseudo-first order model, respectively. The thermodynamic study confirmed the RBV5R adsorption was endothermic in nature and governed by physisorption process. All these findings signified that the MgAl/LDH-RSSB is a promising adsorbent for treating wastewater containing RBV5R dye.

* Corresponding author.
E-mail address: chazmier@usm.my (M.A. Ahmad).
Peer review under responsibility of King Saud University.

Production and hosting by Elsevier

https://doi.org/10.1016/j.arabjc.2023.104643

1. Introduction

Throughout the world, water pollution is considered as one of the most unlikely environmental problems and researchers are in desperate need to find solutions (Vieira, 2009). In the East Coast Region of Peninsular Malaysia, "batik" is among the most popular textile industries. The growing demand of "batik" industry had significantly contributes towards Malaysia's economic development (Bello et al., 2012). In a typical "batik" making industry, pigments or dyes including direct, reactive, basic, acid, disperse, sulphur and solvent dyes are used as starting material to colour the cotton fabric (Hameed et al., 2007). Unfortunately, huge amount of contaminated wastewater is being produced which contain mostly dyes, toxic compounds, and caustic dissolved solids (McKay and Sweeney, 1980). It has been reported that at least, 10 % of the dyestuff will remain in the water stream as wastes (Bello and Ahmad, 2011).

Remazol Brilliant Violet 5R (RBV5R) is a type of reactive dye and known as one of most applied dyes especially in textile making industry (Khasri et al., 2021). It has been extensively used in fabric making production due to its high solubility in water, low energy consumption in the dyeing process, and simple application techniques (Hanafi and Sapawe, 2020). RBV5R falls under the azo dyes which contain usually-one or more azo groups structurally. It is the largest class (above 60 %) among all commonly used dyes in textile industry. As reported, the total dye production was 7×10^7 tons (Chen et al., 2013). So, 60 % of it is considered as azo dyes which accumulates into 42,000,000 tons of dyes. Therefore, the amount of azo dyes (RBV5R) being disposed into the water bodies are 15 % x 42,000,000 tons, which equal to 6,3000,000 tons of azo dyes (Ayed et al., 2011)– (Thangaraj et al., 2021). In terms of the application, RBV5R can also act as initiator used during the fabrication of polymer dyes. It is also an anthracene derivative and therefore is it categorized under the important class of toxic substances and recalcitrant organic contaminants (Bello and Ahmad, 2011). The exposure of RBV5R into the water stream are seriously harmful and dangerous. Presence of RBV5R in the ecosystem caused toxic environment to the living aquatic organisms, preventing the penetration of sunlight and finally results in inhibition of direct photosynthesis process (Bello and Ahmad, 2011). Besides, RBV5R is also toxic, mutagenic, and carcinogenic to humans, fish species and microorganisms (Thitame and Shukla, 2016). RBV5R has a very stable conjugate structure and due to this properties, it is challenging to be removed either by sludge adsorption of biodegradation (Li, 2017). Therefore, an efficient method for decreasing and eliminating the RBV5R from textile industrial effluent before its being discharged into the water stream is crucial.

Several technological methods had been applied for treating the wastewater containing RBV5R dye which includes, chemical coagulation (Kim et al., 2004), photocatalytic degradation (Chong et al., 2010); (Zangeneh et al., 2015), Fenton oxidation (Holkar et al., 2016), anion exchange (Zhu, 2016), biodegradability (Al-Momani et al., 2002) and electrochemical oxidation (Li et al., 2014). Unfortunately, these technologies are costly, only efficient under low dye concentrations, time consuming and generates toxic by-products. Considering all the introduced alternative approach, adsorption process is known as the most reliable method because it is practical, easy to conduct, efficient and reusability of adsorbent is possible (Ma, 2012)– (Yu, 2015). Finding a suitable adsorbent that is inexpensive and at the same time, having high efficiency can be challenging. For now, various types of adsorbents have been explored with the purpose of removing dyes from industrial textile effluent. Researchers have also showed continuous interest to developed adsorbents with excellent adsorption capacity (Amin et al., 2020).

Lately, the implementation of layered doubled hydroxide (LDHs) for removal of coloured wastewater are becoming popular. LDHs are anionic clays and it is a form of inorganic layered compound. Rapid development of LDHs are mainly due to the easy preparation method, high surface area and superb interlayer anion exchangeability (Deng et al., 2018). LDHs have been used in different sorts of applications as polymer nanocomposites (Gu et al., 2015), adsorbents (Zhang et al., 2014); (Mustapha Bouhent et al., 2011), catalyst (Youn et al., 2015); (Sahoo et al., 2011), catalyst support (Xie et al., 2014)–(Ballarin, 2012), drug carried (Kuo, 2015), electrodes (Memon, 2014), and flame retardant (Wang, 2013). This inorganic layered compounds are illustrated by the chemical formula $[M_{1-x}^{2+} M_x^{3+} (OH)_2]^{x+} (A^{n-})_{x/n} \cdot mH_2O$, where M^{2+} is divalent metal cations (M^{2+} = Mg^{2+}, Ni^{2+} Co^{2+} Cu^{2+}, Zn^{2+} and others) and M^{3+} is the trivalent metal cations (M^{3+} = Al^{3+}, Fe^{3+}, Cr^{3+} and others), whereas A^{n-} is the interlayer exchangeable anions including NO_3^-, CO_3^{2-}, SO_4^{2-}, Cl^-, Br^-, I^- and others, and m is the quantity of water molecules (Mandal et al., 2009); (Xia et al., 2015). LDHs function by exchanging the composition of interlayer anions and also the di- and trivalent cations depending on the applications (Bharali and Deka, 2017). However, the main downside of using LDHs alone is that they are unable to regenerate. Besides, they are not highly resistant towards continuous testing activity (Meili, 2019). Therefore, LDHs can be supported with larger particle materials such as biochar in order to enhanced the efficiency of LDHs (Wang et al., 2016).

The performance of LDHs can be enhanced by compositing bi and trivalent metals on the carbon materials such as biochar. Biochar is a carbon rich material that has a stable compound. It is produce through thermal decomposition of biomass under oxygen deficient condition (Lehmann, 2007). Biochar is highly favourable compared to the other available carbon materials (carbon nanotubes, graphene, and ordered mesoporous carbon) since the biomass feedstock are easily obtainable, abundant, and low in cost. The feedstock usually comes from various sources including municipal solid waste materials, agricultural and forest wastes, industrial by-products and wastes, and nonconventional materials (Inyang, 2016). Table 1 show the various selection of biomass feedstock. Besides, biochar properties having high degree of carbon porosity, high surface area and rich with surface functional groups (Amin et al., 2020); (Srivatsav et al., 2020) making it versatile to be used in different sorts of application such as bioenergy production, energy storage, carbon sequestration, biomass waste management, soil amendment (Hou et al., 2020)– (Rahman et al., 2020) and heavy metals removal (Kim et al., 2019). Other than that, biochar had also been extensively applied in treating dye wastewater effluent (Lehmann, 2007).

Currently, microalgae-based biochar had been produced and applied for the mitigation of carbon dioxide (CO_2) via photosynthesis, contributing towards the reduction of Greenhouse Gases (GHGs) in the atmosphere. Besides, it is also being utilized as an attractive source for carbon capture technology (Law, 2022). Lam et al. (Lam, 2020) had produced a simplified and efficient method using microwave assisted technology for the development of palm shell activated biochar. The developed biochar was used for hazardous landfill leachate treatment (Lam, 2020). Considering all the advantages of biochar, it has a very high potential to be introduced on the LDH. Hence, the performance of biochar-LDH towards dye removal can be significantly improved.

Malaysia is known for its rubber industry, and it is the 3rd largest manufacture of natural rubber in the world after Thailand, Indonesia and India (Reshad et al., 2018). The rubber industry plays and important role since it contributes towards the country's economy output (Mokhtar et al., 2015). Natural rubber (latex) can be obtained directly from the rubber (*Hevea brasiliensis*) tree. Rubber seed, which is one of the rubber tree by-products is extracted for the oil. Increasing demand from the oil extraction process had consequently produce huge amount of rubber seed shell (RSS). These RSS are usually discarded as wastes and has zero value. To overcome the disposal environmental issue, development of rubber seed shell biochar from raw biomass material would be a better alternative since it is environmentally friendly, and sustainable approach for the conversion of agricultural wastes into worth added product. As a matter of fact, the production of RSS biochar from biomass would not only solve the waste disposal issue but also treating the dye wastewater effluent (Lahijani et al., 2019).

Table 1 Various biomass feedstock selection.

Biomass feedstock	Method of preparation	Type of modification	Refs.
Tobacco stem	Carbonization at 600 °C or 1 h under N_2 condition.	Impregnated with oxalate monohydrate ($K_2C_2O_4{\cdot}H_2O$) and calcium carbonate ($CaCO_3$).	(Zhang, 2022)
Soybean straw	Heated in a muffle furnace under oxygen limited condition at 450 °C for 2 h.	Impregnated with lime ($Ca(OH)_2$)	(Wang, 2022)
Walnut shell	Pyrolyzed in a muffle furnace heated to 600 °C for 2 h under vacuum.	-	(El Hamdouni, 2022)
Citrus peel	Pyrolyzed under different temperatures (500 °C, 600 °C, 700 °C, 800 °C) under N_2 atmosphere.	Soaking with NaOH	(Du, 2022)
Watermelon rind	Pyrolyzed in a furnace reactor at different temperatures (200, 300, 400, 500, 600 °C).	Impregnated with zirconyl solutions ($ZrOCl_2{\cdot}8H_2O$)	(H. Hoang Phan Quang, , 2022)
Rice straw, eucalyptus leaves and vetiver grass	Pyrolyzed in a muffle furnace filled with nitrogen at 400 °C temperature for 2 h.	-	(Dai, 2021)
Coconut shell	Slow pyrolysis at 450 °C for 2 h.	Treated with phosphoric acid (H_3PO_4)	(Baharum et al., 2020)
C. oleifera shells	Pyrolyzed under N_2 condition with heating temperature of 500–900 °C.	Impregnated with magnesium oxide	(Xu et al., 2022)
Wheat straw Rice straw	Pyrolyzed in a muffle furnace equipped with digital temperature controller under N_2 condition.	-	(Manna et al., 2020)
Root of rose *(Rosa damascene)* and stem of eucalyptus *(Eucalyptus citriodora)*	Pyrolyzed in a fixed bed furnace at 450 °C	-	(Khare et al., 2017)

Nadarajah *et al.* (Nadarajah et al., 2018), had investigated the rhodamine B removal from aqueous solution using rubber seed shells (*Hevea Brasiliensis*) as adsorbent. To the best of the author's knowledge, still there has been no studies on the MgAl/layered double hydroxide supported on rubber seed shell biochar for Remazol Brilliant Violet 5R removal. In fact, this is the novel and first experimental study performed using MgAl/LDH derived rubber seed shell (*Hevea Brasiliensis*) biochar for the removal of RBV5R dye. Therefore, this research study focuses on the development of rubber seed shell (RSSB) and investigating the potential of incorporating MgAl/LDH onto the RSSB surfaces to enhance the anionic RBV5R dye removal. Besides, the kinetics, thermodynamics, and isotherms study of the RBV5R dye adsorption onto MgAl/LDH-RSSB biochar was analysed. A schematic diagram explaining the RBV5R adsorption mechanism by MgAl/LDH-RSSB adsorbent has also been investigated.

2. Materials and methods

2.1. Materials

Magnesium nitrate hexahydrate ($Mg(NO_3)_2{\cdot}6H_2O$) and aluminium nitrate nonahydrate ($Al(NO_3)_3{\cdot}9H_2O$) which are the LDH precursor salts, was purchased from Merck (USA). Cloramphenicol ($C_{11}H_{12}C_{12}N_2O_5$) (adsorbate), sodium hydroxide (NaOH) (alkali pH adjuster), and hydrochloric acid (HCl) (acidic pH adjuster), was purchased from Sigma Aldrich (USA). The purity of all these chemicals was 98 %. All chemicals were used as it is without any further modification.

2.1.1. Preparation of rubber seed shell biochar (RSSB)

Rubber seed shells (*Hevea brasiliensis*) was obtained from Serdang's rubber tree plantation region which is located at Perak (GIS: 5.194152, 100.586235). The shells were scrubbed and dry off overnight at 105 °C oven temperature. Then, the dried rubber seed shells were pulverized into the 1–2 mm particle size using laboratory mechanical crusher. After that, the shells were pyrolyzed using a vertical carbonization rig for 90 min and 150 ml/min nitrogen flowrate and 20 °C/min heating rate. To investigate the effect of pyrolysis temperature, rubber seed shells were pyrolyzed at 500 °C, 700 °C, and 900 °C. The range of selected pyrolysis temperature of rubber seed shell biochar are chosen based on the previous published manuscript (Reshad et al., 2018). Table 2 shows the proximate composition of rubber seed shell biomass.

2.1.2. Preparation of MgAl/LDH-RSSB

MgAl/LDH-RSSB was synthesized using co-precipitation method. 1 mol of magnesium nitrate hexahydrate ($Mg(NO_3)_2{\cdot}6H_2O$) and 1 mol of aluminium nitrate nonahydrate ($Al(NO_3)_3{\cdot}9H_2O$) were added into a 200 ml beaker containing 100 ml deionized water. The solution was stirred vigorously for 30 min at 60 °C until complete dissolution. Then, in a separate 500 ml beaker, 1 g of RSS biochar was weighed, and the prepared dissolution was added. The mixture was shaken continuously and 3 mol/l of NaOH was dropwise until the solution reached pH 10. Then, the solution was stirred vigorously for 24 h at 65 °C. After that, the co-precipitation solution was centrifuged and washed with 1000 ml of deionized water for 5 times to remove remaining impurities. The obtained MgAl/LDH-RSSB was subsequently dried for 16 h in the oven at 85 °C.

3. Analytical study

Various characterization technique had been implemented to determine the elemental composition, BET surface area, sur-

face morphology, and surface functional groups of the prepared RSSB and MgAl/LDH-RSSB adsorbent.

3.1. Elemental analysis

The ultimate analysis was conducted to determine the percentage of carbon, hydrogen, nitrogen, sulphur, and oxygen (by difference) in the biomass and biochar RSS samples. The elemental composition of those samples was determined using an elemental analyser (PerkinElmer Series II 2400, USA model). The samples were combusted in an oxygen-rich environment at 975 °C. The separation of carbon, hydrogen, nitrogen, and sulphur fraction was performed using the gas chromatography (GC) column, whereby helium was used as the carrier gas.

3.2. Nitrogen adsorption–desorption

A nitrogen adsorption/desorption volumetric gas adsorption instrument (Micrometrics, ASAP 2020 Series, Germany) was used to determine the BET surface area, total pore volume, mesopore volume, micropore volume, and average pore diameter of RSSB and MgAl/LDH-RSSB. Before the analysis, about 0.1 g of each sample was placed in an analysis tube and degassed at 300 °C for at least 5 h. This procedure was done to remove any adsorbed species from the surface. After completing the degassing part, the sample was transferred to the analysis station where it was cooled in liquid nitrogen environment at 77 K. A software linked to an analyzer was used to automatically monitor the adsorption–desorption process.

3.3. Scanning electron microscope (SEM)

SEM analysis was carried out to study the surface morphology of the prepared RSSB and MgAl/LDH-RSSB samples. A Leo Supra 55VP Microscope, Field Emission, Germany model machine was used to perform the analysis. The selected sample was placed on an aluminium stab with a double-sided carbon tape. Then, it was scanned at different magnifications.

Table 2 Proximate composition of rubber seed shell biomass.

Parameter	Value
Proximate analysis (wt%, dry basis)	
Volatiles	77.70
Ash	0.40
Fixed carbon	21.90

3.4. Fourier transform infrared spectroscopy (FTIR)

A Shimadzu Prestige 21, Japan model spectroscopy was used to record the infrared spectra of the selected RSSB (pristine) and MgAl/LDH-RSSB samples between 500 cm^{-1} to 4000 cm^{-1} wavenumbers at 1 cm^{-1} resolution. The spectra were the results of four scans at a speed of 1 scan/2 s. The FTIR spectra of selected RSSB (pristine) and MgAl/LDH-RSSB samples were recorded by preparing the potassium bromide (KBr) pellets. The KBr together with the adsorbent sample was ground and pelletized to a size of approximately 1.3 cm. The obtained transparent and thin pellet was later placed in a sample holder for analysis.

3.5. Adsorption activity of remazol brilliant violet 5R (RBV5R)

Batch adsorption tests were conducted in 500 ml Erlenmeyer flasks. Initially, the RBV5R stock solution (1000 ppm) was formulated by dissolving 1000 mg of RBV5R dye with 1000 ml of deionized water in a volumetric flask. The prepared 1000 ppm stock solution was later diluted to a certain initial concentration. After that, 250 ml of known solution concentration was poured into the 500 ml Erlenmeyer flask. Then, 0.2 g of the prepared MgAl/LDH-RSSB was added into the RBV5R solution. Different parameter conditions including initial RBV5R concentration (25, 50, 100, 200, 250 and 300 mg/l), adsorption temperature (30, 45 and 60 °C), and pH were studied to further enhance the RBV5R removal. After 24 h, the concentration of the adsorbate (RBV5R) solution was detected using UV–vis Spectrophotometer at 577 nm maximum wavelength. The adsorption capacity and removal of RBV5R can be obtained using the following Eq. (1) and Eq. (2), respectively:

$$qe, adsorption = \frac{V(C_{i-}C_e)}{M} \quad (1)$$

$$R(\%) = \frac{(C_i - C_e)}{C_i} x100 \quad (2)$$

whereby q_e,adsorption (mg/g) is the quantity of RBV5R adsorbed per gram of adsorbent (MgAl/LDH-RSSB) at equilibrium (mg/g), R ($\%$) represents the percentage of RBV5R removal efficiency, C_i and C_e (mg/l) are the initial RBV5R concentrations in the solution at equilibrium, V (l) is the RBV5R solution volume, and M represents the adsorbent (MgAl/LDH-RSSB) mass (g).

4. Results and discussion

4.1. Characterization of MgAl/LDH-RSSB

4.1.1. Ultimate analysis of the RSS biomass and biochar samples

In this research study, rubber seed shell (RSS) had been chosen as the biomass feedstock to produce biochar. The selection of

Table 3 Ultimate analysis value for the prepared RSS samples.

Sample	Ultimate analysis (wt %)				
	Carbon	Hydrogen	Nitrogen	Sulfur	Oxygen*
RSS biomass	47.56	6.40	0.20	0.42	45.42

* Calculated by difference.

RSS is based on the abundant availability, zero costing, efficiency (Monteiro et al., 2017) and also the proximate and ultimate analysis value as shown in Table 1. It can be observed that raw rubber seed shell has high carbon content of 47.56 % and low ash content of 0.40 % (Anthonysamy et al., 2020) (value taken from previous work). These two properties are considerably important in order to obtained the best quality of biochar, having high adsorption capacity uptake, high adsorbent surface area and good mechanical strength (Oliveira et al., 2016); (Kaghazchi and Soleimani, 2006). Besides, the low sulphur content in both raw (0.42 %) and biochar (0.05 %) samples are highly beneficial since it can reduce the discharge of sulphur dioxide gas which consequently produces acid rain (Rashidi et al., 2012).

As seen in Table 3, the carbon content in RSS biochar is higher than the raw RSS with 50.13 %. During the carbonization process, more volatile compounds are being released from the raw materials and it is converted into certain gases such as carbon monoxide (CO). As a result, biochar with high carbon content and percentage yield is being produced (Borhan and Yusuf, 2020). According to the literatures, the best carbon content for selection of the raw material is around 40–80 % (Guarín Romero et al., 2018). Therefore, rubber seed shell has the potential to be used as the source of biomass feedstock to produce biochar.

Table 4 The porosity structures of RSSB and MgAl/LDH-RSSB.

Properties	RSSB	MgAl/LDH-RSSB
BET surface area (m^2/g)	114.32	132.40
Total pore volume (cm^3/g)	0.0617	0.0732
Mesopore volume (cm^3/g)	0.0136	0.0220
Micropore volume (cm^3/g)	0.0481	0.0512
Average pore diameter (nm)	2.16	2.21

4.1.2. Porosity properties and surface morphology

The porous characteristics of pristine (RSS biochar) and modified (MgAl/LDH-RSSB) are shown in Table 4. Based on Table 4, the BET surface area of RSS biochar is low 114.32 m^2/g. Incorporating the LDH metals into the RSS biochar surfaces improved the porous structure, whereby the BET

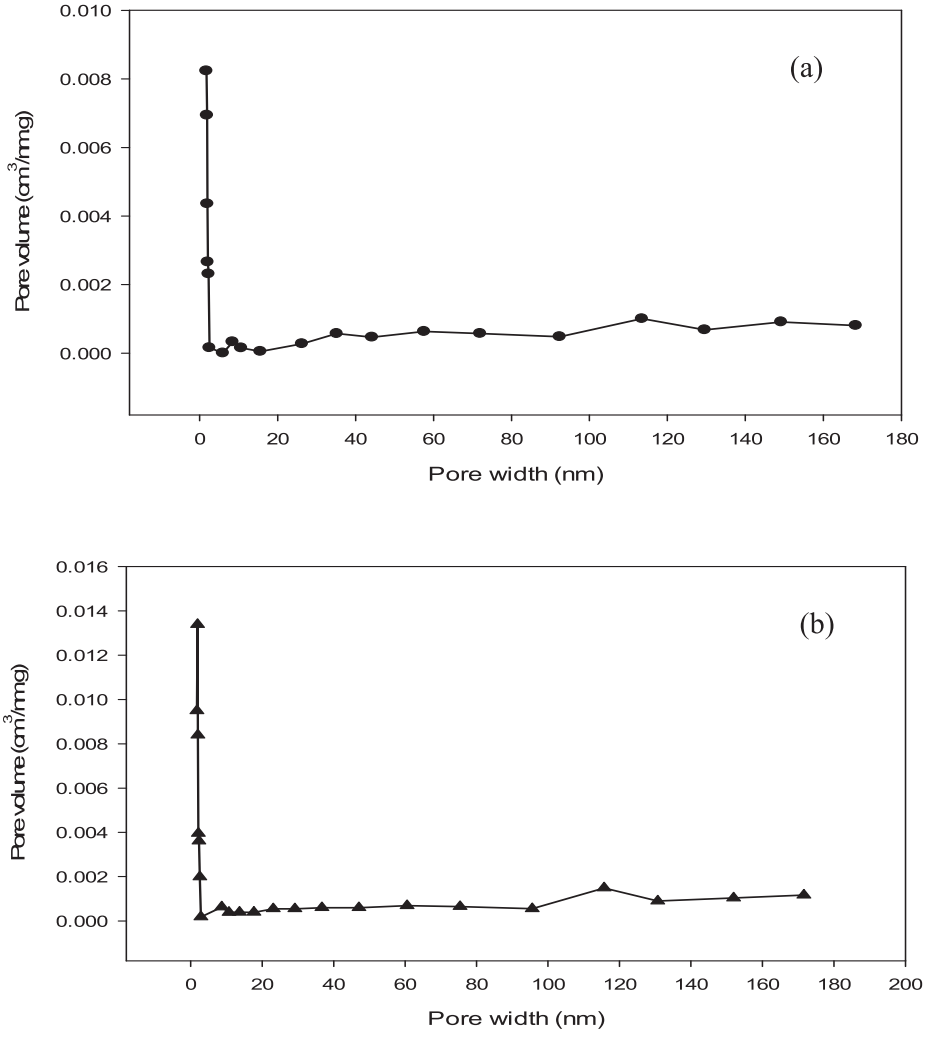

Fig. 1 Pore size distribution of (a) RSSB and (b) MgAl/LDH-RSSB.

surface area increases up to 132.40 m^2/g. Besides, most of the adsorbent surfaces in both samples are occupied with microporous structure. Around 77.96 % and 69.95 % from the total pore volume comprises of micropores in MgAl/LDH-RSSB and RSSB, respectively. The pore size distribution of RSSB and MgAl/LDH-RSSB is display in Fig. 1 (a) and (b), respectively. Based on Fig. 1, the pore diameter distribution for both RSS biochar and MgAl/LDH-RSSB falls between 1.72 nm and 171 nm. This indicates that both pristine and modified adsorbents consist of mainly micropores, mesopores and few macropores. The average pore diameter for RSS biochar and MgAl/LDH-RSSB is 2.16 nm and 2.21 nm, respectively.

The surface morphology of pristine (RSS biochar) and modified (MgAl/LDH-RSSB) were analysed using scanning electron microscopy. SEM images of RSS biochar and MgAl/LDH-RSSB at different magnification is shown in Fig. 2. As observed in Fig. 2 (a) and (b), the surface texture in RSSB is highly porous but hollow. During the carbonization process of RSS, most of the volatile compounds are being released hence, more open pore structures are formed on the surface of RSS (Borhan and Yusuf, 2020). After co-precipitating the RSSB with MgAl/LDH, abundant micropores honey-comb structure had been developed on the surface of MgAl/LDH-RSSB. As a result, the RBV5R molecules was directly adsorbed onto the micropore surfaces of MgAl/LDH-RSSB. Besides, the pores are filled with LDH particles as shown in Fig. 2 (c) and (d). This observation agrees with the BET and pore distribution results. Similar finding has been reported by Wu *et al.* (2017), whereby the modified biochar (MB) also shows presence of more micropore structure on the adsorbent surfaces as compared to the original biochar (OB) (Wu and Feng, 2017).

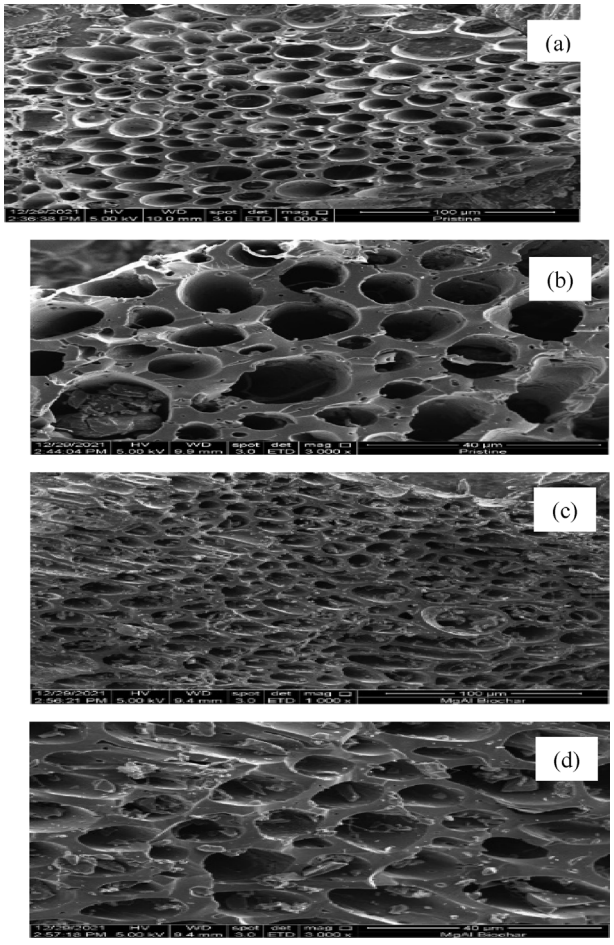

Fig. 2 Scanning electron microscopy images of RSSB (a, b: 1000x, 3000x). MgAl/LDH-RSSB (c, d: 1000x, 3000x).

4.1.3. Fourier transform infrared (FTIR) spectroscopy surface functionality

Fig. 3. shows the FTIR spectra for both RSSB (pristine) and MgAl/LDH-RSSB. As observed in Fig. 3, the adsorption bands at 3382 and 1645 cm^{-1} wavenumber which exist in the MgAl/LDH-RSSB are associated to O—H and H—O—H stretching vibrations. The hydroxyl groups appeared mainly due to the presence of water molecules found in the middle layer of the adsorbent and might be also due to the water molecules that is being physically adsorbed (Zhang et al., 2013); (Li, Jul. 2016). A small peak was detected at 1628 cm^{-1} wavenumber in the biochar sample. This peak represents the O—H stretching vibration of alcohol, water, carboxylic acid and phenol, which present in the pyrolyzed RSSB (pristine) sample. Besides, it also represents the loss of water from the surface of the adsorbed solids on the outer surface of the crystalline structure (Fonts et al., 2009). A significant peak observed around 1364 cm^{-1} in the MgAl/LDH-RSSB may be assigned to the corresponding asymmetric CO_3^{2-} stretching vibration. This signifies the presence of contaminated carbonate group from the environmental air and accumulates in the intermediate layer of the MgAl/LDH-RSSB (Zhang et al., 2013); (Liu et al., 2007). A small band detected at 1019 cm^{-1} wavenumber in the biochar sample is associated to the C—O—H binding group. A peak around 650 cm^{-1} is related to the Al-O and Mg-O stretching vibrations band, representing the cations which are formed in the MgAl/LDH-RSSB (Abdellaoui et al., 2017); (Djebbi, 2016).

4.2. Effect of environmental factors

At the beginning of this research study, a preliminary test (Figure S1) for optimizing the parameters of the adsorbent (MgAl/

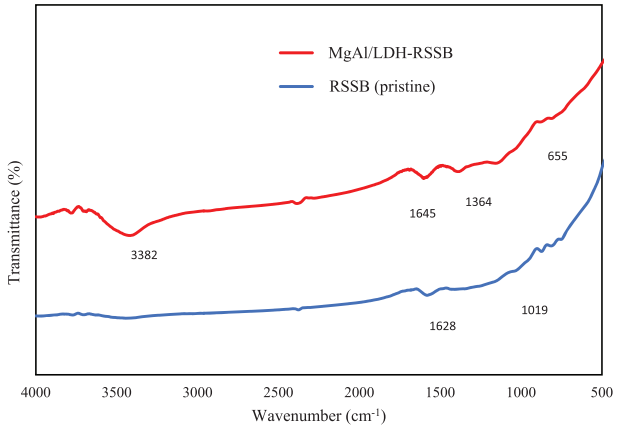

Fig. 3 FTIR spectroscopy of RSSB (pristine) and MgAl/LDH-RSSB.

LDH-RSSB) had been performed using one factor at a time (OFAT) method. Different preparation condition including biochar pyrolysis temperature (500, 700 and 900 °C), MgAl/LDH ratio (1:1, 2:1, and 3:1), and biochar ratio (0.5 g, 1 g and 1.5 g) was study to obtain the maximum RBV5R uptake capacity. Based on the results in Figure S1, the optimum preparation condition for MgAl/LDH-RSSB was at 700 °C of biochar pyrolysis temperature, 2:1 of MgAl/LDH ratio and 1 g of biochar ratio. To study the other batch adsorption parameters, the optimum MgAl/LDH-RSSB condition will be used throughout this experimental activity.

4.2.1. Effect of initial dye concentration and contact time

The influence of RBV5R initial dye concentration (25–300 mg/l) and contact time (0–24 h) towards RBV5R uptake capacity and removal by MgAl/LDH-RSSB at various adsorption temperature (30, 45 and 60 °C) was studied and display in Fig. 4,5 and 6. Other parameters including the adsorbent dosage (0.2 g) and solution pH (5.5) were remained constant. As seen in Fig. 4 (a), Fig. 5 (a) and Fig. 6 (a), the RBV5R adsorption capacity increases linearly with time from 14.53 mg/g to 52.33 mg/g, 20.78 mg/g to 85.99 mg/g and 23.75 mg/g to 125.88 mg/g at 30, 45 and 60 °C, respectively as the initial concentration of

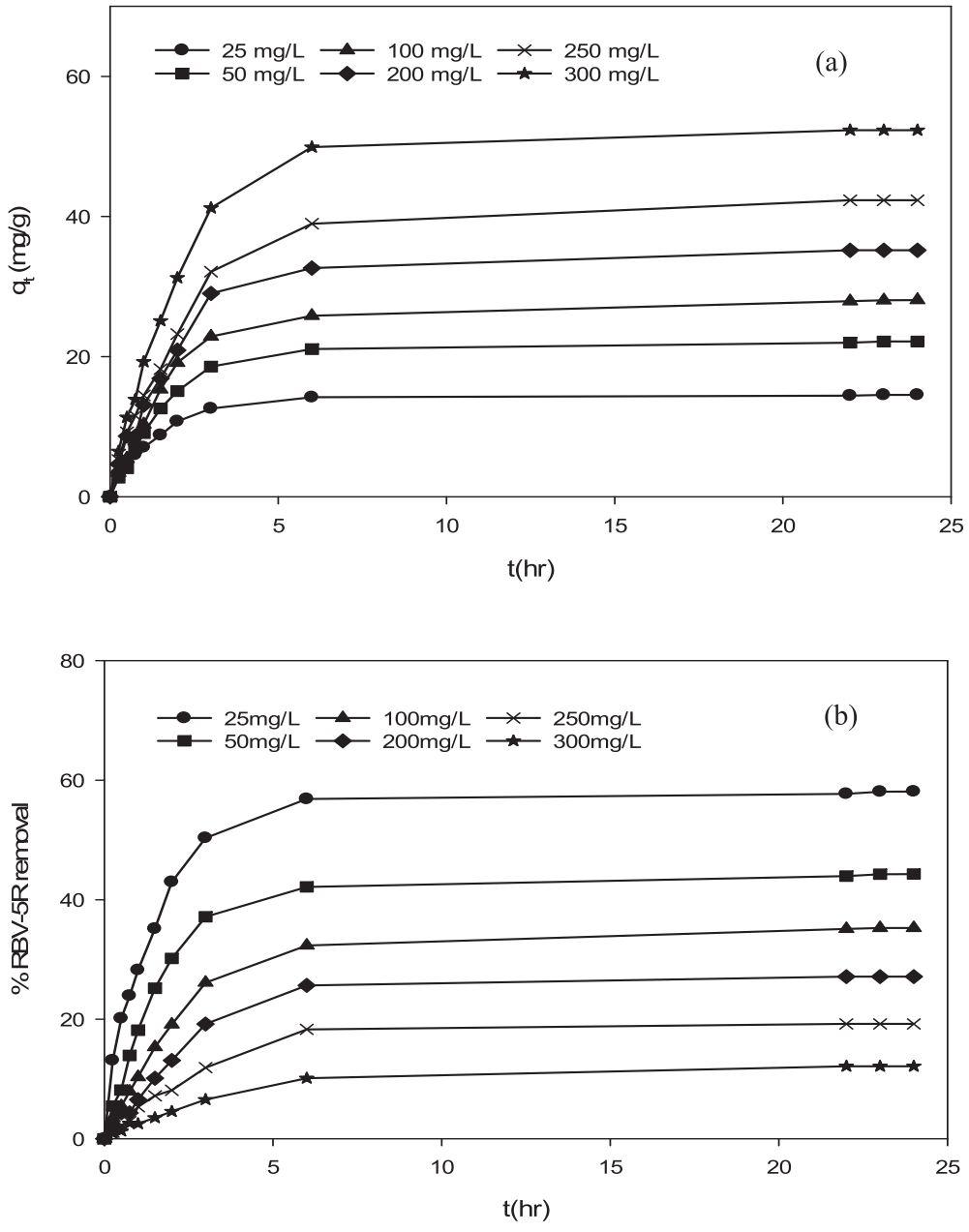

Fig. 4 Effect of RBV5R initial concentration and contact time towards RBV5R (a) adsorption capacity and (b) percentage removal by MgAl/LDH-RSSB at 30 °C adsorption temperature.

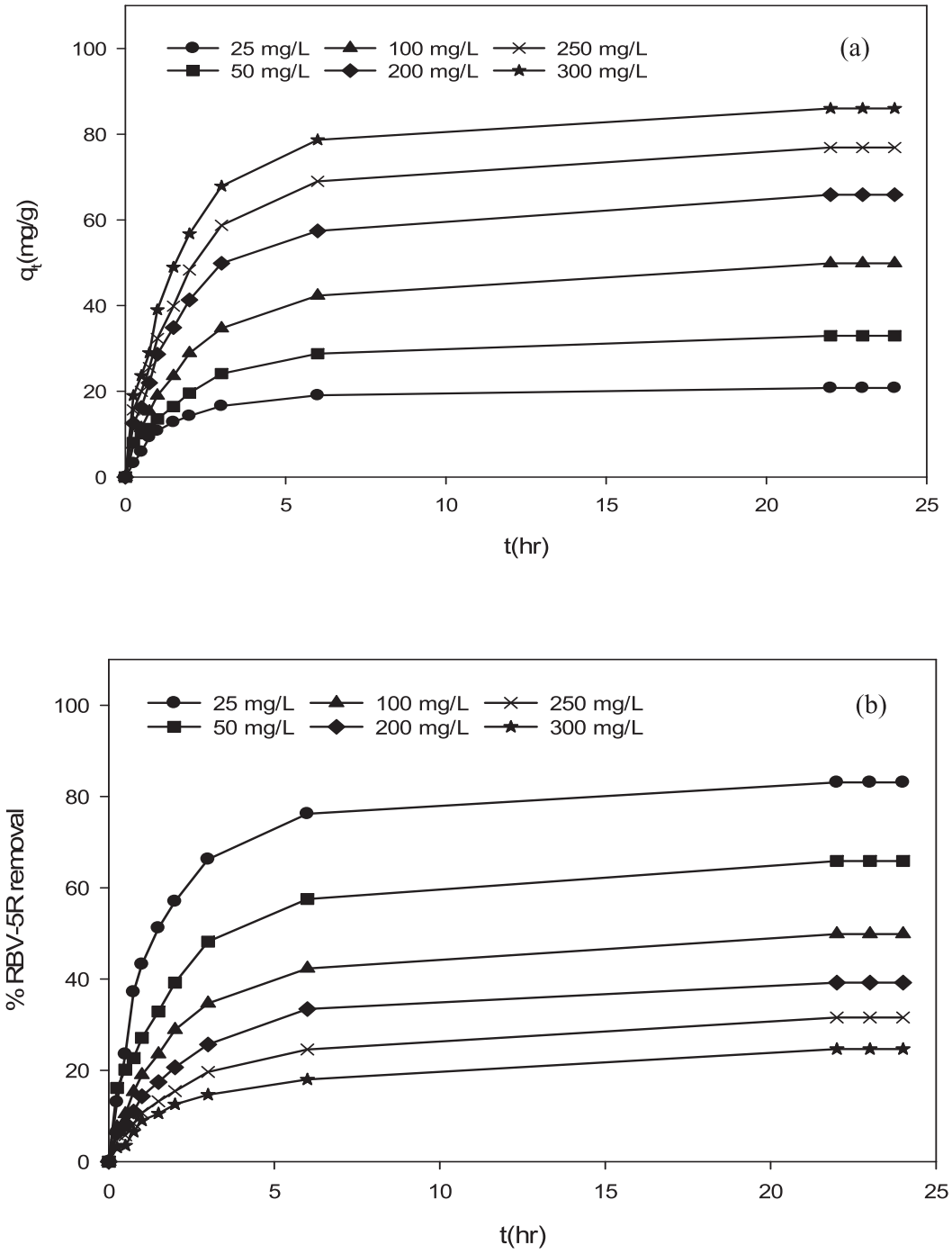

Fig. 5 Effect of RBV5R initial concentration and contact time towards RBV5R (a) adsorption capacity and (b) percentage removal by MgAl/LDH-RSSB at 45 °C adsorption temperature.

RBV5R increases from 25 to 300 mg/l. In contrast, the RBV5R removal decreases from 58.12 to 12.13 %, 83.12 to 24.66 % and 94.99 to 38.89 % at 30, 45 and 60 °C, respectively. Based on Figs. 4, 5 and 6, the adsorption capacity was found to be fast at the beginning phase (first 4 min) of the adsorption period and then the uptake became slower as it reaches the equilibrium state (within 24 h). This occurrence was associated with the presence of more available vacant surface sites for adsorption process. As a result, higher adsorption uptake capacity was observed due to strong electrostatic attraction between anionic species of RBV5R in the aqueous solution and surfaces of MgAl/LDH-RSSB (Zubair et al., 2021).

After 20 h, the remaining availability surface active sites decreases and difficult to be occupied as the RBV5R adsorp-

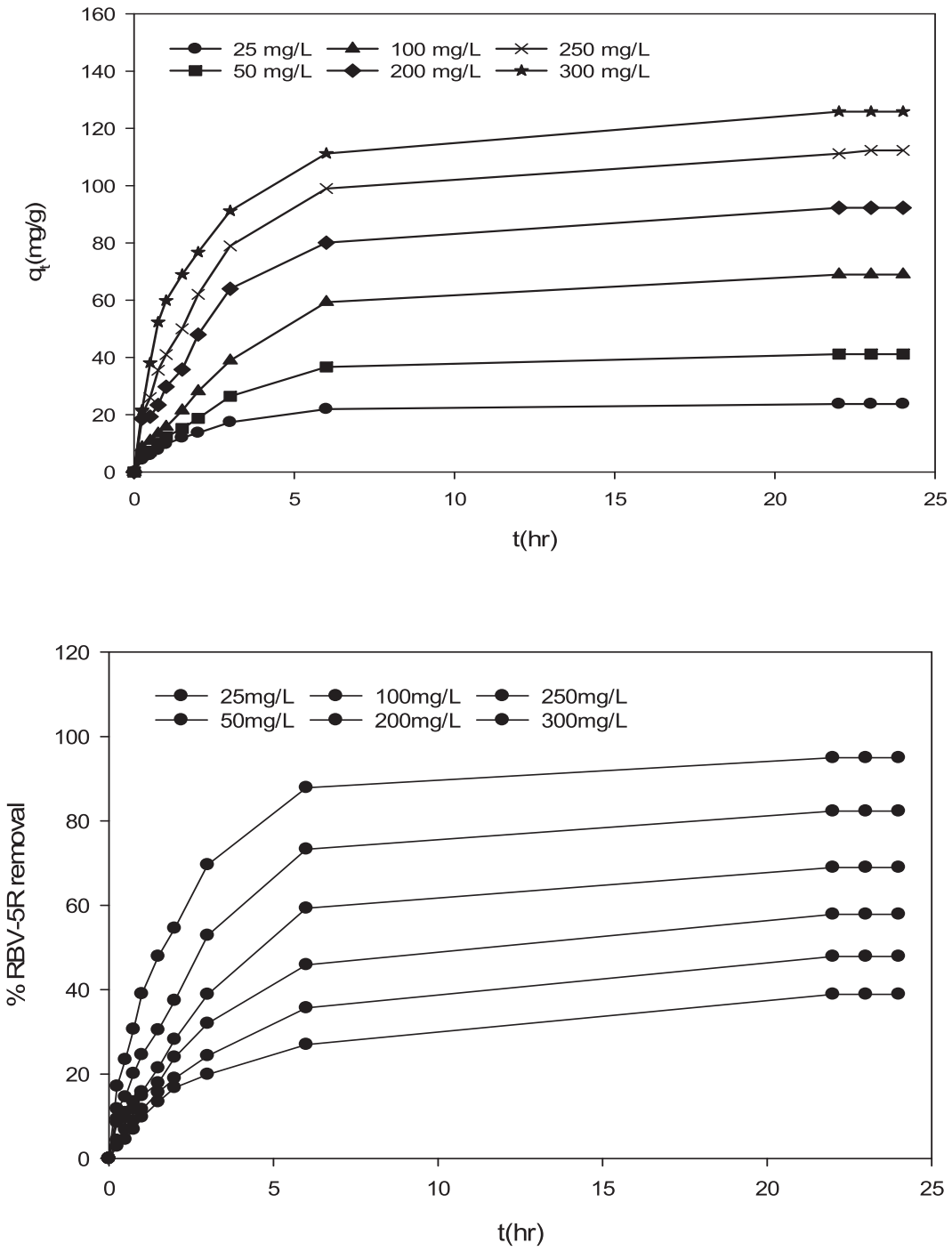

Fig. 6 Effect of RBV5R initial concentration and contact time towards RBV5R (a) adsorption capacity and (b) percentage removal by MgAl/LDH-RSSB at 60 °C adsorption temperature.

tion capacity uptake decreases by MgAl/LDH-RSSB. This was mainly due to the repulsive forces occurred among the RBV5R solute molecules and solid surfaces MgAl/LDH-RSSB (Hameed and a a Ahmad, 2009). Therefore, the adsorption process had reached its saturation point within 24 h at all RBV5R concentrations (25 mg/l-300 mg/l). Similar studies have been reported by Khasri et al. (Khasri et al., 2021), whereby the RBV5R adsorption uptake by melunak and rubberwood sawdust based activated carbon increased rapidly at the initial stage signifying strong electrostatic attractions taking place among the RBV5R dye and adsorbent surfaces 19.61 mg/g to 151.50 mg/g and 19.20 mg/g to 150.02 mg/g, respectively as initial dye concentration of RBV5R increases from 25 to 300 mg/l. Thereafter, no remarkable changes on the adsorption capacity was observed as the adsorption process had reached its equilibrium stage (Khasri et al., 2021). Bello et al. (Bello et al., 2012) had reported that the amount of RBV5R adsorbed at equilibrium time indicates the maxi-

mum adsorption capacity of an adsorbent (Bello et al., 2012). At the beginning of the adsorption activity, RBV5R dye molecules had to pass through the layer film barrier, then penetrate into the adsorbent surfaces, and finally diffuse into the adsorbent pores (Senthilkumaar et al., 2005).

4.2.2. Effect of adsorption temperature

In this part, effect of solution temperature (30, 45, and 60 °C) on RBV5R uptake capacity by MgAl/LDH-RSSB at various initial RBV5R concentrations (25 to 300 mg/l) was investigated. Fig. 7 shows the results of RBV5R equilibrium uptake capacity at 30, 45 and 60 °C adsorption temperature. As observed from Fig. 7, the adsorption capacity for RBV5R was found to enhanced from 14.53 mg/g to 52.33 mg/g, 20.78 mg/g to 85.99 mg/g and 23.75 mg/g to 125.88 mg/g, respectively, as the adsorption temperature increased from 30 °C to 60 °C. This occurrence signifies that the RBV5R adsorption process by Mg/Al/LDH-RSSB was endothermic in nature. Besides, the diffusion rate between RBV5R dye molecules with the internal and external boundary layer pores of MgAl/LDH-RSSB particle increases resulting from the increased in the solution temperature due to the low level of viscosity in the RBV5R solution (Bello et al., 2012).The increased in the RBV5R uptake capacity as the can be also associated with the fact that the RBV5R molecules required sufficient energy to interact with the MgAl/LDH-RSSB surface active site as the solution temperature was increased (Gokulan et al., 2019).

Similar result had been reported by Bello et al. (Bello et al., 2012), whereby the quantity of RBV5R dye increases from 12.99 mg/g, 52.63 mg/g and 76.92 mg/g as the temperature increases from 30 to 60 °C, respectively. In another reported study, Gokulan et al. (Gokulan et al., 2019) has justified the adsorption capacity of RBV5R by *C. Scalpelliformis* derived biochar increases as the temperature of adsorption increases from 20 to 45 °C. The enhancement in terms of the uptake capacity was due to the pore size enlargement on the adsorbent surfaces (Gokulan et al., 2019). Considering the effect of adsorption temperature towards RBV5R adsorption capacity, the optimum temperature for the RBV5R uptake was identified to be at 30 °C.

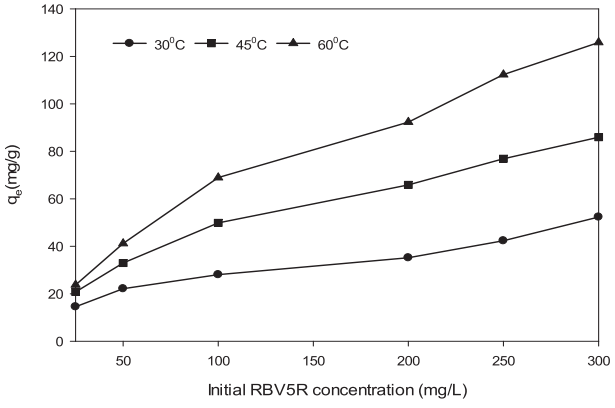

Fig. 7 Equilibrium uptake capacity of RBV5R adsorbed by MgAl/LDH-RSSB at various adsorption temperatures (30, 45 and 60 °C).

4.2.3. Effect of adsorption pH

The influence of pH on RBV5R removal by MgAl/LDH-RSSB was studied, and subsequent results are displayed in Fig. 8. The RBV5R percentage removal decreases from 92.7 mg/g, 90.8 mg/g, 89.7 mg/g, 84.8 mg/g, 77.6 mg/g to 74.8 mg/g, respectively as the initial pH increases from pH 2 to pH 12. At lower pH, the adsorbent surface was mainly occupied with positive charge. These positively charged surface ions will eventually attract to the negatively charged functional groups of the RBV5R dye, resulting in high RBV5R removal. As the solution pH increased, the negatively charged adsorbent surfaces also increases. This creates an electrostatic repulsion among RBV5R dye molecules and adsorbent surfaces (Demirbas and Nas, 2009). Hence, the removal of RBV5R was found to be decreasing.

4.3. Mechanism of interaction for RBV5R dye on MgAl/LDH-RSSB

A sequence of isotherm, kinetic, intraparticle diffusion, and thermodynamic studies were conducted to understand the whole adsorption mechanism of RBV5R dye molecules on MgAl/LDH-RSSB surfaces, and the subsequent results are reviewed in the following sections.

4.3.1. Adsorption isotherm models

Several common isotherm models involving Langmuir, Freundlich, Temkin, and Dubinin-Radushkevich have been applied to analyse the isotherm data. The Langmuir isotherm model represents a monolayer adsorption at homogeneous adsorption sites. As shown in Eq. (3), the linearized Langmuir adsorption model can be expressed (Langmuir, 1918):

$$\frac{C_e}{q_e} = \frac{C_e}{q_m} + \frac{1}{q_m K_L} \tag{3}$$

whereby, C_e (mg/l) represents the concentration of RBV5R at equilibrium time, q_e (mg/g) represents the RBV5R adsorption capacity at equilibrium time, q_m (mg/g) represents the single layer adsorption capacity, and K_L represents the Langmuir sorption constant.

To confirm the favourability of the Langmuir model, the dimensionless equilibrium parameter (R_L) defined by Eq. (4) was used (Langmuir, 1916):

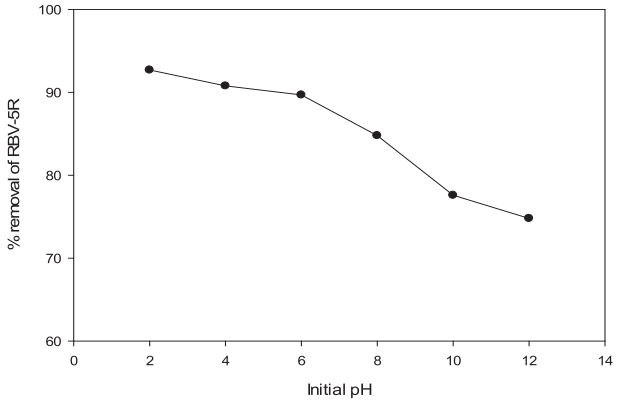

Fig. 8 Percentage removal of RBV5R by MgAl/LDH-RSSB at different pH (2,4,6,8,10 and 12).

$$R_L = \frac{1}{1 + K_L C_0} \quad (4)$$

whereby, C_0 represents the highest initial concentration of RBV5R. The R_L value can be used to decide the favourability of the isotherm data. If ($R_L = 0$), isotherm is considered irreversible. If ($R_L = 1$), isotherm is considered linear. If ($R_L > 1$), isotherm is considered unfavourable.

Freundlich model isotherm signifies the multilayer adsorption that take place on heterogeneous adsorbent surfaces. The linearized form of equation is as shown in Eq. (5) (Freundlich, 1906):

$$\log q_e = \frac{1}{n} \log C_e + \log k_F \quad (5)$$

whereby, C_e (mg/l) and q_e (mg/g) represents the RBV5R concentration and adsorption capacity at equilibrium time, respectively; n represents the adsorption intensity constant and K_F represents the adsorption capacity constant.

Temkin model demonstrate the influence of adsorbate interaction on the adsorbent surfaces. The linearized equation can be expressed as shown in Eq. (6) (Temkin and Pyzhev, 1940):

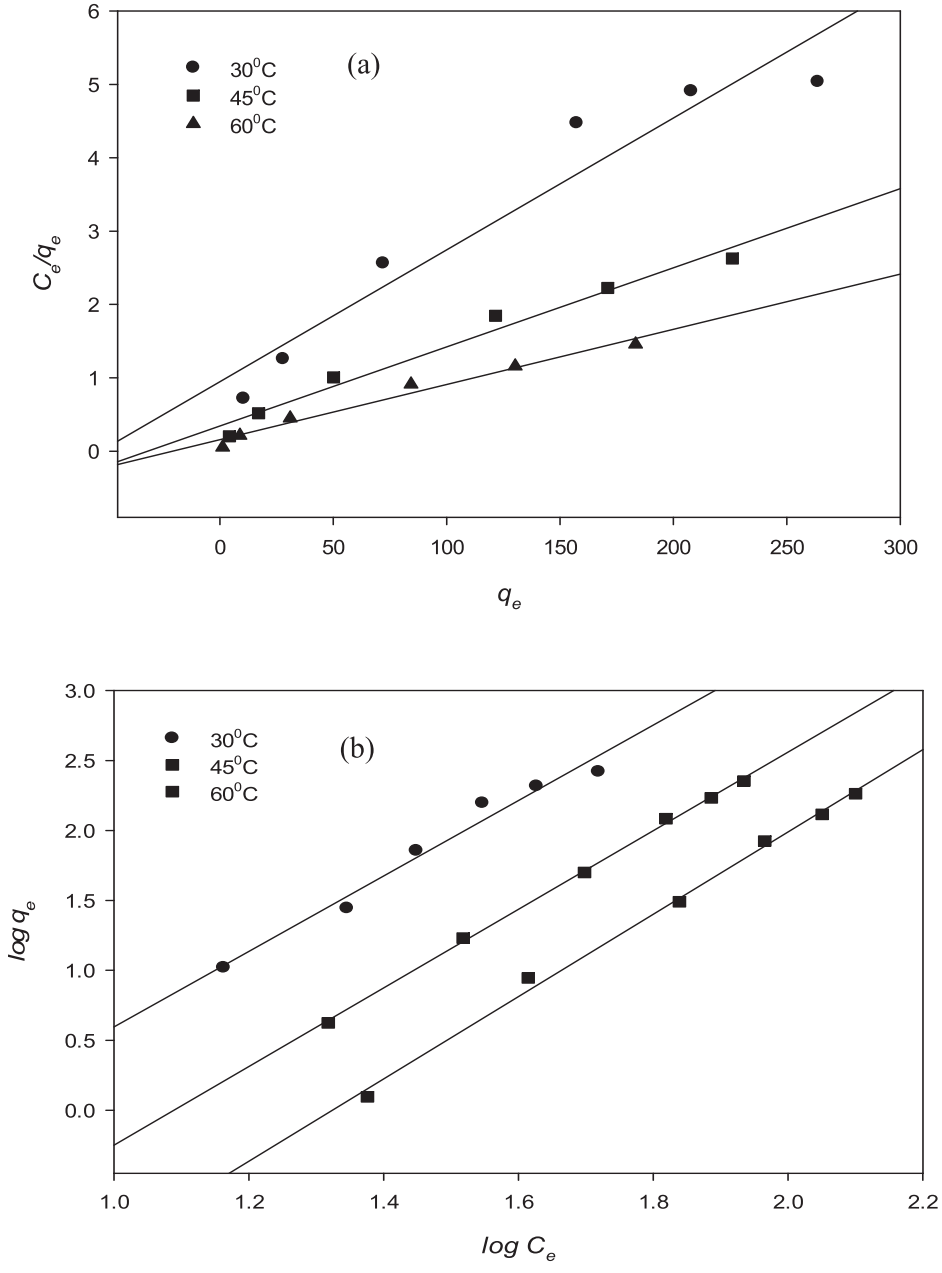

Fig. 9 RBV5R adsorption isotherms: (a) Langmuir and (b) Freundlich by MgAl/LDH-RSSB at 30 °C, 45 °C and 60 °C.

$$q_e = \frac{RT}{b_T}(\ln A_T + \ln C_e) \quad (6)$$

whereby, q_e (mg/g) represents the adsorption capacity at equilibrium time, C_e (mg/l) represents the concentration of RBV5R at equilibrium time; A_T and b_T are the Temkin constants, R (8.314 $J/mol.\ K$) represents the gas constant and T (K) is the temperature.

Dubinin-Radushkevich (D-R) isotherm is applied to study the effect of porous adsorbent structure (Alberti et al., 2012). This isotherm suggests the micropore volume filling are the main factor that affects the adsorption process rather than multilayer adsorption (Inglezakis, 2007). The Dubinin-Radushkevich model is greater than Langmuir isotherm since it does not consider constant adsorption potential or homogenous surface adsorption. The linearized equation can be expressed as shown in Eq. (7) (Kaur et al., 2015):

$$q_e = q_{max} \exp(-\beta\varepsilon^2) \quad (7)$$

whereby, q_e (mg/g) represents the adsorption capacity at equilibrium time, q_{max} (mg/g) represents the maximum adsorption capacity, β ($mol^2 \cdot k/J^2$) represents the constant adsorption energy, and ε (kJ/mol) represents the Polanyi potential; ε can be demonstrate as shown in Eq. (8) (Bharali and Deka, 2017):

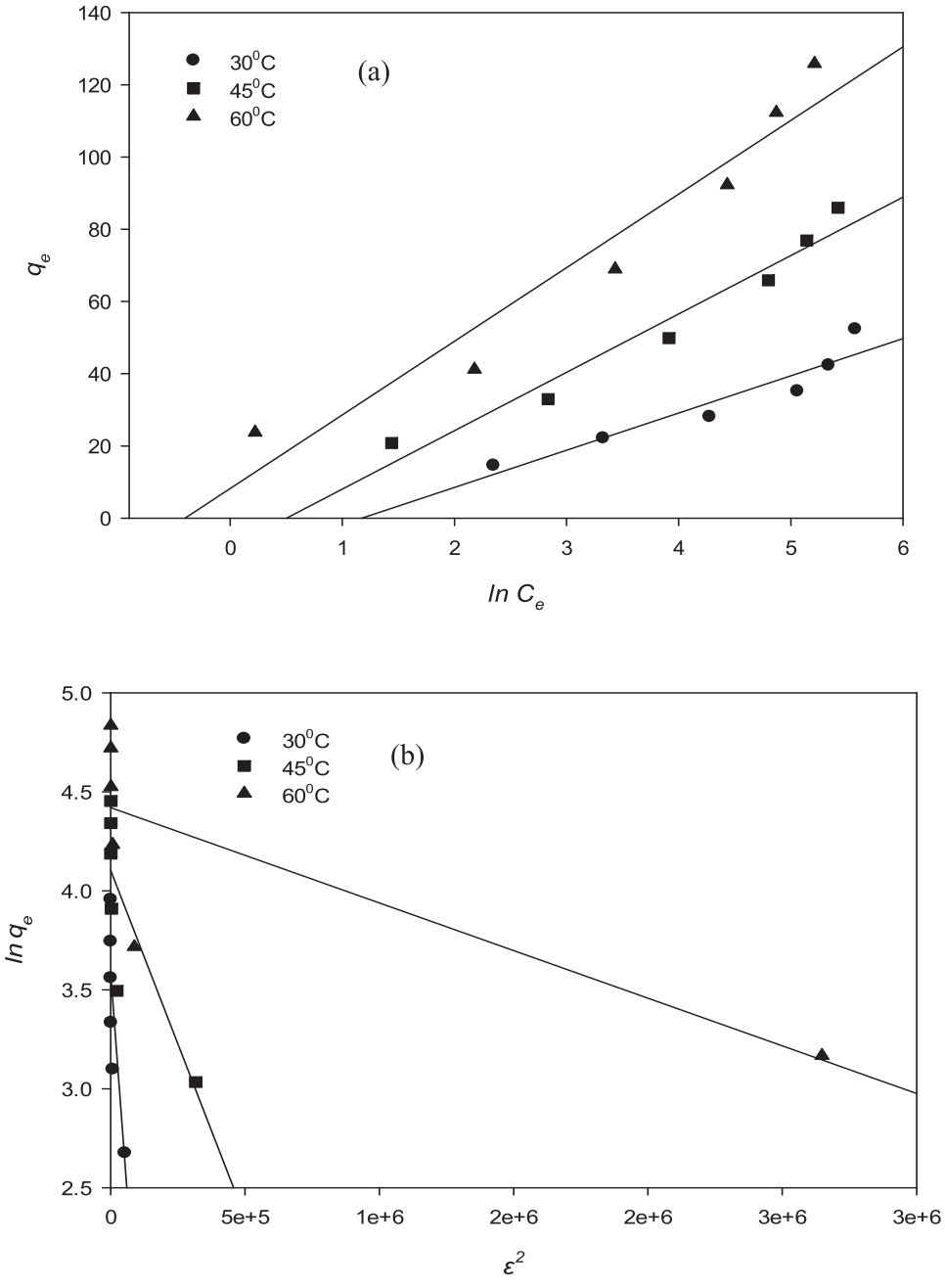

Fig. 10 RBV5R adsorption isotherms: (c)Temkin and (d) Dubinin Radushkevich by MgAl/LDH-RSSB at 30 °C, 45 °C and 60 °C.

$$\varepsilon = RT\ln\left(1+\frac{1}{C_e}\right) \tag{8}$$

whereby, R (8.314 $J/mol.K$) is the universal gas constant and T (K) is the absolute temperature. The adsorption energy, E can be obtained from Eq. (9) (Bello et al., 2012):

$$E = \frac{1}{\sqrt{2\beta}} \tag{9}$$

The E value can be used to determine the adsorption characteristic. If the E value $<$ 8 kJ/mol, the mechanism was mainly governed by physical adsorption. Otherwise, it was controlled by chemical adsorption (Helfferich, 1962).

Fig. 9 (a), (b) and Fig. 10 (a), (b), illustrates the RBV5R adsorption isotherm (Langmuir, Freundlich, Temkin, Dubinin-Raduchkevich (D-R) of MgAl/LDH-RSSB at various temperatures (30 °C, 45 °C, 60 °C). The corresponding parameters and correlation coefficients calculated from linear isotherm model equations are presented in Table 5. At 30 °C, 45 °C, 60 °C, the equilibrium isotherm data was determined to be fitted by the Freundlich model, and the correlation coefficient value was close to 1; R^2 = 0.9736, R^2 = 0.9988, R^2 = 0.9958 at 30 °C, 45 °C, 60 °C, respectively, as compared to the Langmuir model. Table 5 depicts how the k_f and n values indicates the heterogeneity of the material as well as the potential of RBV5R adsorption on the surfaces of the MgAl/LDH-RSSB. Additionally, the values of $1/n$ are observed to be <1; n = 0.3611, n = 0.3556, n = 0.338 at 30 °C, 45 °C, 60 °C, respectively, indicating that the adsorption of RBV5R onto MgAl/LDH-RSSB is favorable (Bello et al., 2012). To analyze the interaction effect between adsorbate and adsorbent, the adsorption equilibrium data was also applied to the Temkin isotherm model (Helfferich, 1962). As seen in Table 5, the value of b_T and A_T increases from 0.3093 to 0.6676 l/mg and 10.307 to 20.392 kJ/mol, respectively as the temperature of adsorption increased from 30 °C to 60 °C. This signifies that the interaction among the adsorbate and adsorbent increase with increase in temperature. As a result, higher adsorption uptake capacity was observed as the energy increases (Bello et al., 2012). The Dubinin-Radushkevich (D-R) isotherm model was used to identify the nature of the adsorption process. It could be controlled either by physical or chemical adsorption depending on the adsorption energy (E) value. Table 5 shows the value of E ranging from 0.7071 kJ/mol to 2.3461 kJ/mol at adsorption temperature (30 °C to 60 °C). From the D-R model, E value was $<$ 8 kJ/mol. Therefore, the uptake capacity of RBV5R dye by MgAl/LDH-RSSB was governed mainly by physical adsorption process (Helfferich, 1962).

4.3.2. Adsorption kinetic models

Various kinetic models containing pseudo first-order, pseudo second-order, Avrami and Elovich were applied to determine the possible uptake mechanism of RBV5R onto the MgAl/LDH-RSSB surfaces. A non-linear regression technique was used to calculate kinetic model parameters and correlation coefficients through Sigma Plot (Version 14.0, USA). Figs. 11-16 and Table 6-8 illustrate the kinetic plot and parameter values at different adsorption temperatures (30 °C, 45 °C, 60 °C).

Pseudo first-order kinetic model is used to describe the physisorption process. This model state that adsorbate and solid surface interact in reversible ways. This can be deduced from the Lagergren rate equation, as shown in Eq. (10) (Chen et al., 2014):

$$\frac{dq_t}{d_t} = k_1\,(q_e - q_t) \tag{10}$$

whereby, k_1 (1/min) represent the first-order rate constant, q_e (mg/g) represent the adsorption capacity at equilibrium and q_t (mg/g) represent the adsorption capacity at a specific time. Integrating Eq. (10) when q_t = 0 at t = 0 and q_t = q_e at t = t_∞ gives the exponential form:

$$q_t = q_e\,(1 - e^{-k_1 t}) \tag{11}$$

Pseudo second-order kinetic model is applied to investigate the chemisorption process and the possible chemical interactions take place between the adsorbent solid surfaces and adsorbate. The model equation can be expressed as shown in Eq. (12) (Kudahi et al., 2017):

Table 5 Isotherm parameters and coefficient correlations for RBV5R dye by MgAl/LDH-RSSB.

Isotherm model	Parameters	Adsorption temperature		
		30 °C	45 °C	60 °C
Langmuir	$q_{e\ exp}$ (mg/g)	52.33	85.99	125.88
	q_{max} (mg/g)	55.56	92.59	133.33
	K_L (l/mg)	0.0190	0.0315	0.0478
	R_L	0.3319	0.2443	0.1833
	R^2	0.9304	0.9768	0.9753
Freundlich	k_F (l/g)	2.2193	2.9722	3.7644
	$1/n$	0.3611	0.3556	0.3384
	R^2	0.9736	0.9988	0.9958
Temkin	A_T (l/mg)	0.3093	0.6061	0.6676
	b_T (kJ/mol)	10.307	16.175	20.392
	R^2	0.901	0.9565	0.9341
Dubinin-Radushkevich	q_m (mol/g)	60.5882	36.0678	83.1462
	E (kJ/mol)	0.7071	0.2236	2.3461
	R^2	0.6643	0.684 0	0.6425

$$\frac{dq_t}{d_t} = k_2 (q_e - q_t)^2 \quad (12)$$

whereby, k_2 (g/mg.min) represent the second-order rate constant, q_e (mg/g) represent the adsorption capacity at equilibrium and q_t (mg/g) represent the adsorption capacity at a given time. According to this model, the uptake rate is linearly related to the square of the number of vacant adsorption sites. Integrating Eq. (12) when $q_t = 0$ at $t = 0$ and $q_t = q_e$ at $t = t_\infty$ gives the exponential form:

$$q_t = \frac{q_e^2 k_2 t}{1 + q_e k_2 t} \quad (13)$$

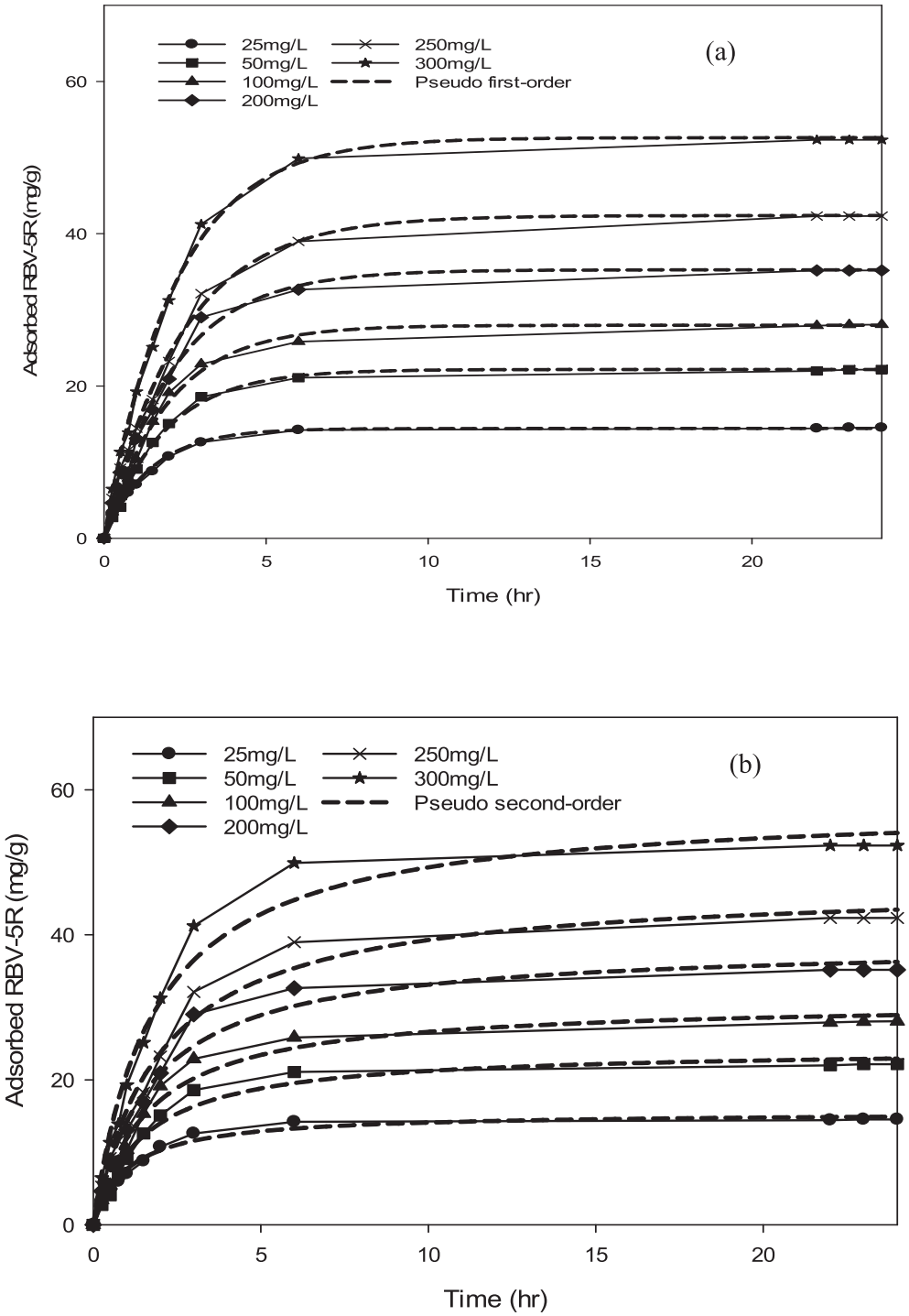

Fig. 11 RBV5R adsorption kinetics: (a) pseudo first-order and (b) pseudo second-order by MgAl/LDH-RSSB at 30 °C.

Avrami model is applied to predict whether the adsorption process was controlled mainly by both physisorption and chemisorption, particularly in modified carbon based adsorbents, as shown in Eq. (14) (Lahijani et al., 2018):

$$\frac{dq_t}{d_t} = k_A^{n_A} t^{n_A{}^{-1}}(q_e - q_t) \tag{14}$$

whereby, $k_A(\min^{-1})$ represent the Avrami kinetic constant, n_A represent the Avrami exponent and it is usually shown in the form of fraction, q_e (mg/g) represent the adsorption capacity at equilibrium and q_t (mg/g) represent the adsorption capacity at a given time. The integrated form of Eq. (15) is:

$$q_t = q_e\,(1 - e^{-(k_A t)n_A}) \tag{15}$$

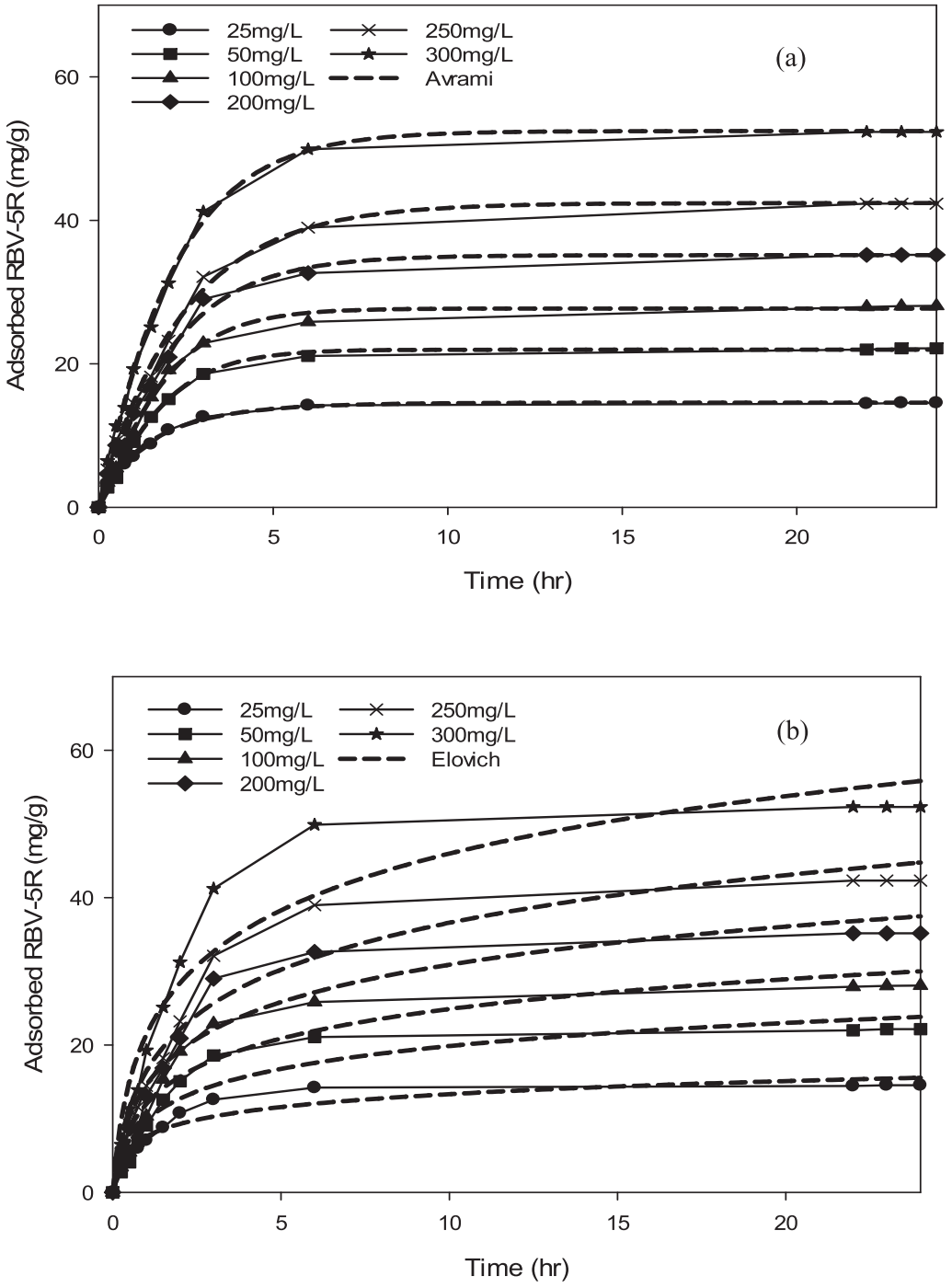

Fig. 12 RBV5R adsorption kinetics: (a) Avrami and (b) Elovich by MgAl/LDH-RSSB at 30 °C.

Another useful model is the Elovich kinetic model, which describes the chemisorption of adsorbate onto solid based adsorbents without product desorption. This model suggest that as the surface coverage increases with time, the reaction rate may decrease (Juang and Chen, 1997):

$$\frac{dq_t}{d_t} = \alpha exp(-\beta q_t) \tag{16}$$

whereby α (mg/g.min) and β (g/mg) represent the model Avrami model constants and q_t (mg/g) represent the adsorption capacity at a given time. As $d\ q_t/dt$ approaches α when $q_t = 0$, it can be considered as the initial reaction rate. Integrating Eq. (16) when $q_t = 0$ at $t = 0$ and $q_t = q_e$ at $t = t$ gives the exponential form:

$$q_t = (1/\beta)\ln(1 + \alpha\beta t) \tag{17}$$

As shown in Table 6-8, the adsorption of RBV5R was best fitted with pseudo first-order at all adsorption temperatures (30 °C, 45 °C, 60 °C), whereby the kinetic model shows good linearity ($R^2 > 0.99$). Besides, the $q_{e,\ cal}$ (calculated) and $q_{e,\ \exp}$ (experimental) values were in good agreement with < 1 %

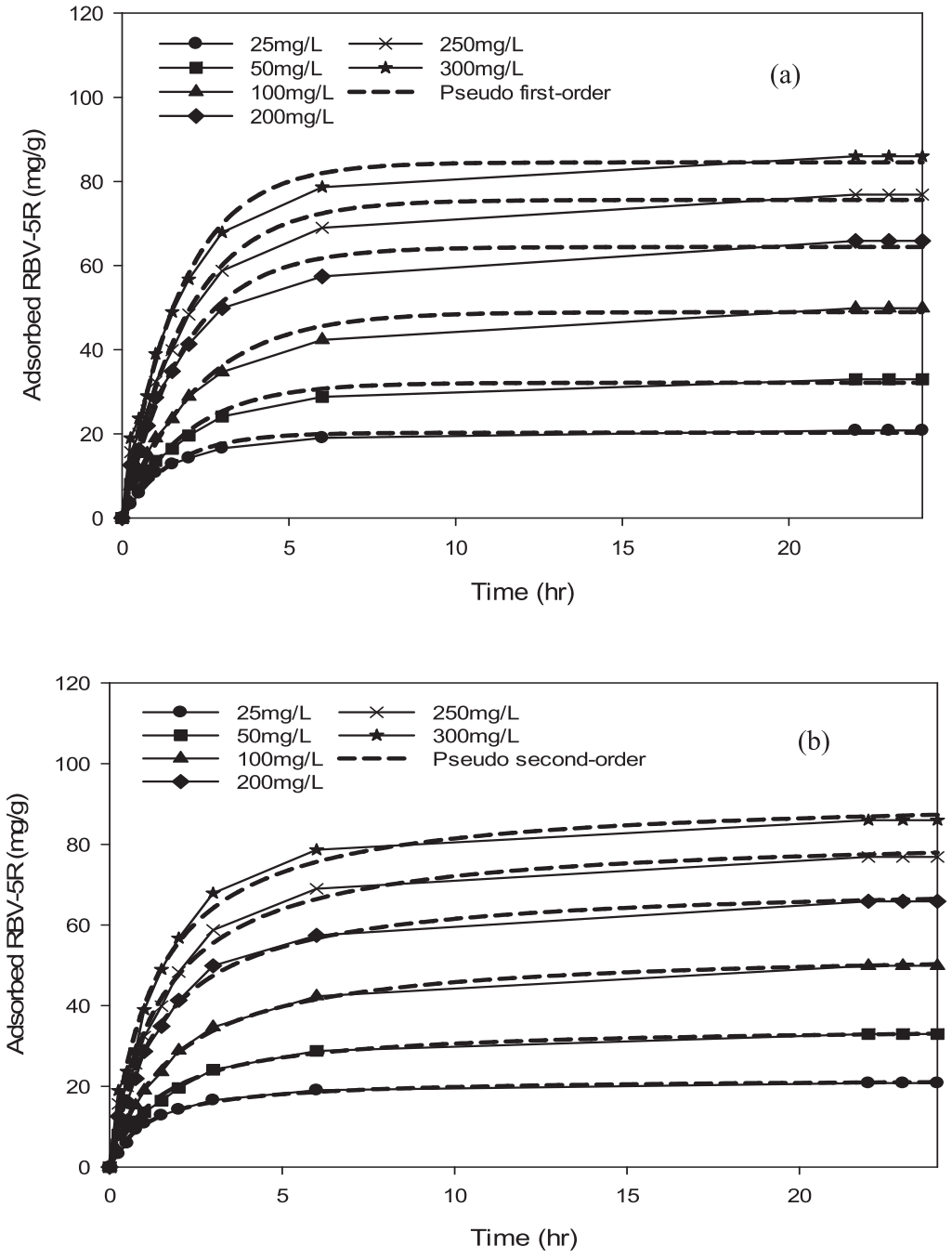

Fig. 13 RBV5R adsorption kinetics: (a) pseudo first-order and (b) pseudo second-order by MgAl/LDH-RSSB at 45 °C.

of deviation. Therefore, physisorption are the main governed mechanism that controls the adsorption of RBV5R by MgAl/LDH-RSSB.

4.3.3. Intraparticle diffusion

The intraparticle diffusion were further investigated using the Weber-Morris particle diffusion model (Kumar and Jena, 2016) to study the diffusion of RBV5R dye molecules onto the prepared MgAl/LDH-RSSB adsorbent at 30 °C, 45 °C, and 60 °C as shown in Figs. 17, 18, and 19, respectively. As can be seen from Figs. 17, 18, and 19, multi-linear lines had appeared with three different regions spotted on the plot, indicating that the intraparticle diffusion was not the sole rate limiting step involved in the adsorption process of RBV5R dye molecules. The initial stage (0 to 1.22 (t^0.5)), starting from the origin, represent the transfer of RBV5R dye molecules from bulk iquid to the external surface of the MgAl/LDH-RSSB adsorbent. The second stage (1.22 to 1.73 (t^0.5)) signifies intraparticle diffusion. The final stage (1.73 to 4.90 (t^0.5)) indicates the equilibrium phase (Wang, 2018). Based on Table 9-11, the k_{ti} values for all three regions increased as the RBV5R initial dye concentration increased. Higher k_{ti} values were obtained due to the greater driving force for mass transfer that developed at higher initial concentrations. Apart

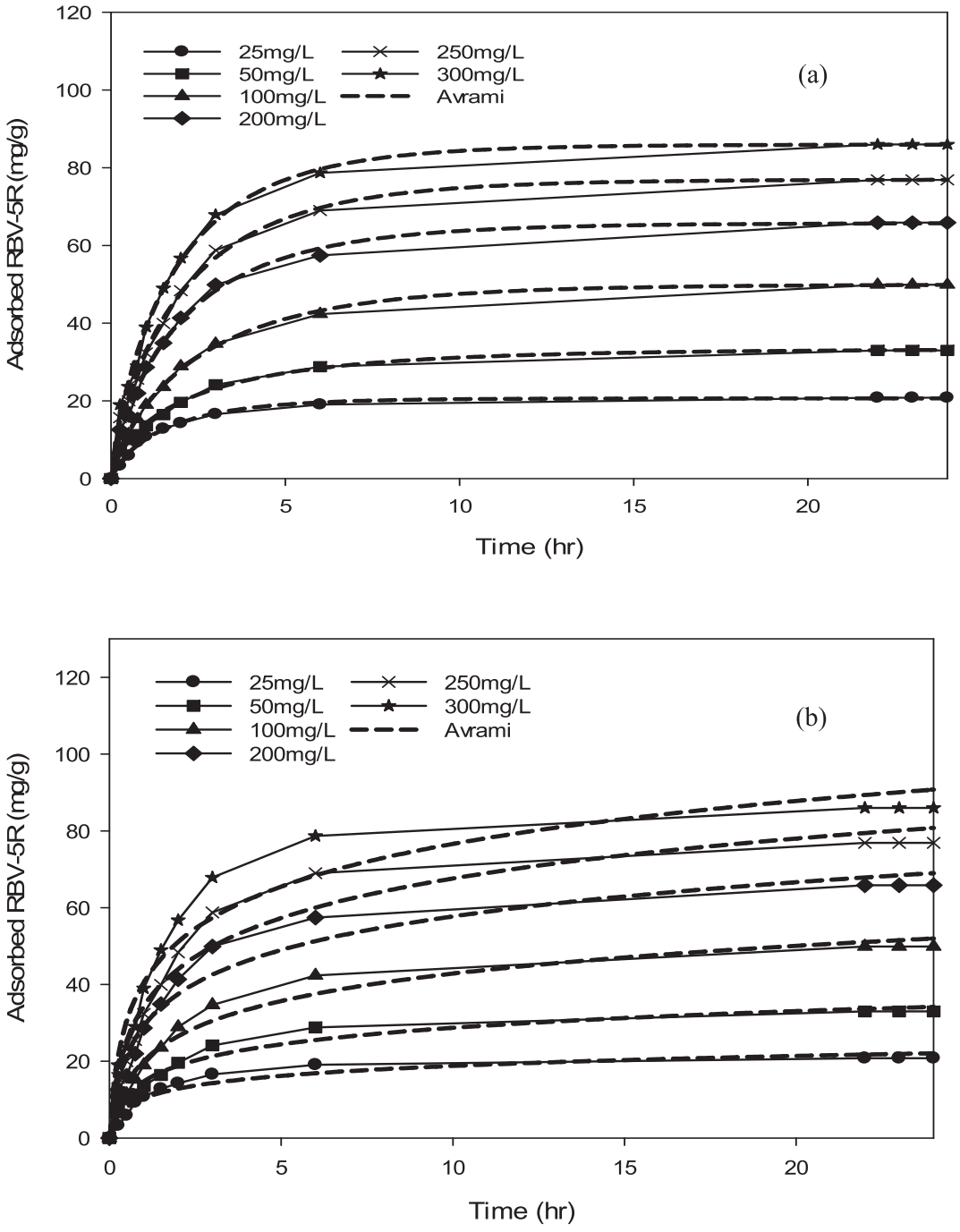

Fig. 14 RBV5R adsorption kinetics: (a) Avrami and (b) Elovich by MgAl/LDH-RSSB at 45 °C.

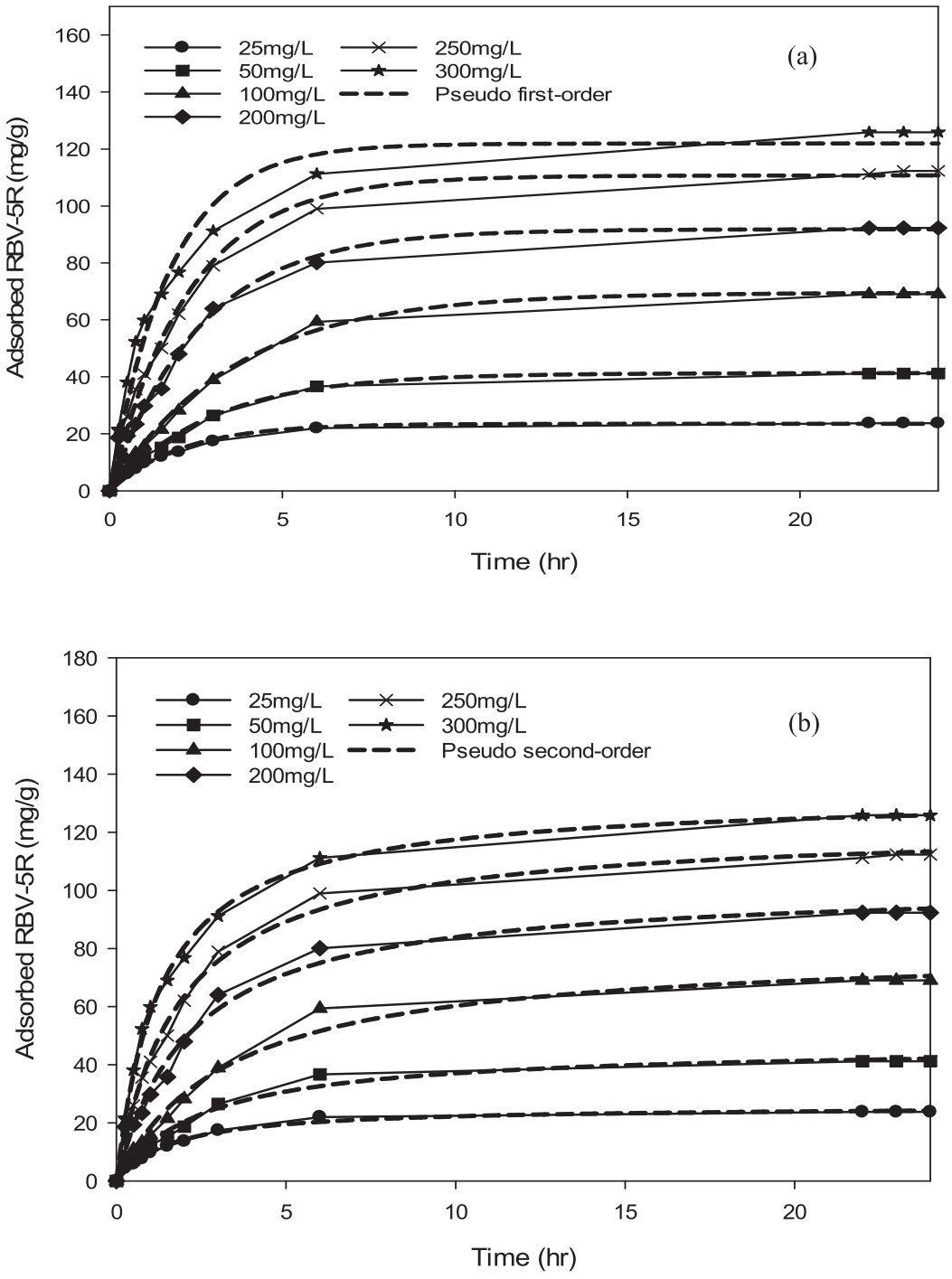

Fig. 15 RBV5R adsorption kinetics: (a) pseudo first-order and (b) pseudo second-order by MgAl/LDH-RSSB at 60 °C.

from the k_{ti} values, it was observed that the values of C_i were found to increase too at higher initial RBV5R dye concentrations in all three regions. Thus, confirming an increase in the boundary layer thickness. Similar observation has also been reported by Khasri et al. (Khasri et al., 2021).

5. Thermodynamic study

In this section, the thermodynamic study had been performed at temperature ranging from 303 K – 333 K and at RBV5R initial concentration between 25 ppm –300 ppm. The calculated $\Delta H°$ (standard enthalpy), $\Delta G°$ (standard free energy) and $\Delta S°$ (standard entropy) which represents the thermodynamic parameters can be directly obtained using the following Eq. (18) (Zubair et al., 2021):

$$\ln K_L = \frac{\Delta S^{\circ}}{R} - \frac{\Delta H^{\circ}}{R} \tag{18}$$

whereby, R (8.314 $J/mol.K$) represent the universal gas constant, $T\ (K)$ represent the absolute temperature and K_L (l/mg) represent the Langmuir isotherm constant. The calculated val-

ues of $\Delta H°$ (standard enthalpy) and $\Delta S°$ (standard free energy) can be obtained directly from the slopes and intercepts of the Van Hoff plot of ln K_L versus 1/T (figure not shown). Meanwhile, the $\Delta G°$ can be determined based on Eq. (19) (Zubair et al., 2021):

$$\Delta G^{\circ} = -RTlnKL \tag{19}$$

To evaluate the RBV5R activation energy, which represents the minimum energy required by the reactants for the reaction to occurred can be obtained using the Arrhenius equation as expressed in the following section (Bello et al., 2012):

$$\ln k2 = \ln A - \frac{E_a}{RT} \tag{20}$$

whereby k_2 (g/mg.min) is the rate constant which can be obtained directly from the pseudo-second-order kinetic model, E_a (kJ/mol) is the Arrhenius activation energy and A is the Arrhenius factor. The value of E_a can be obtained from the

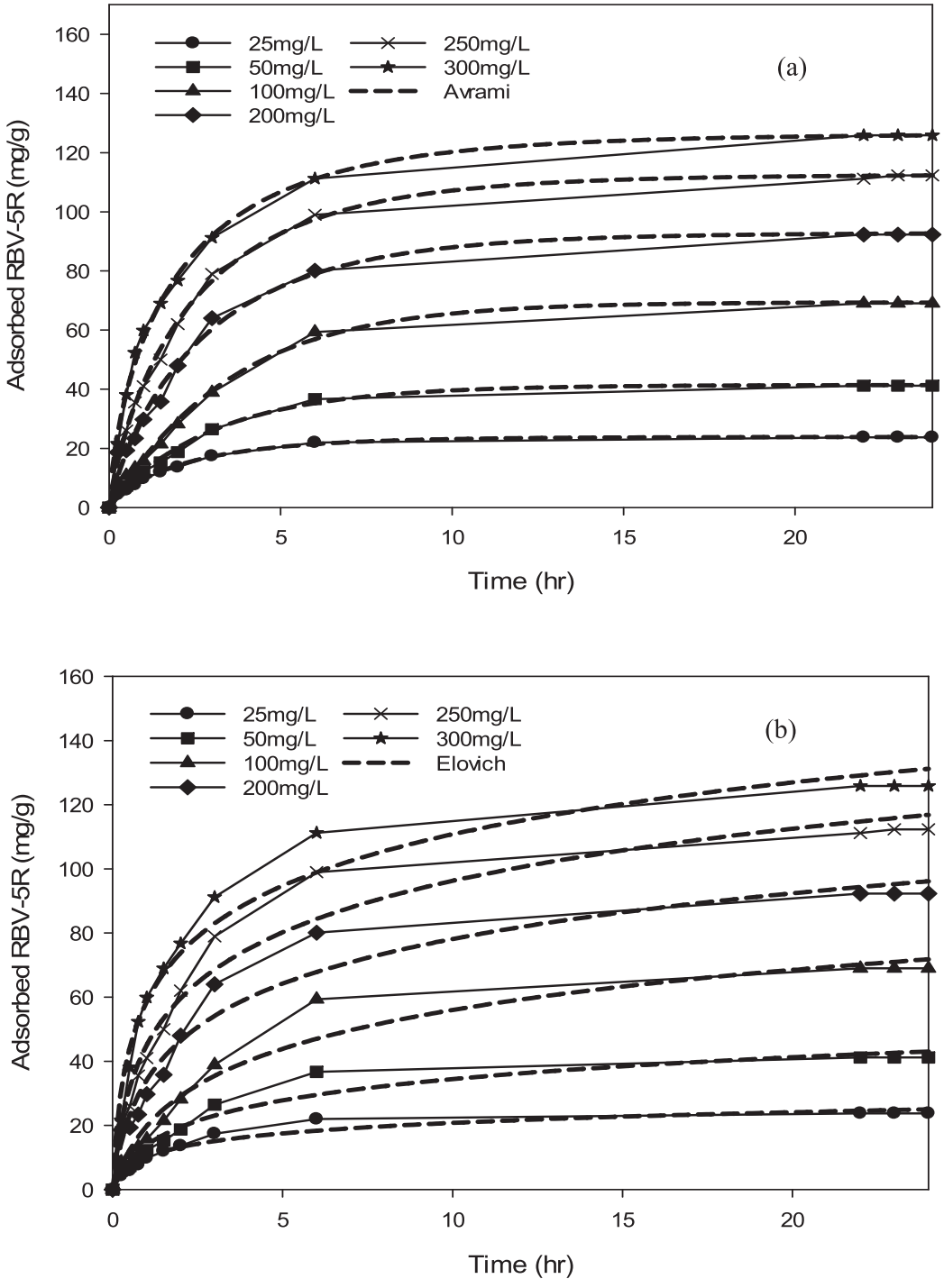

Fig. 16 RBV5R adsorption kinetics: (a) Avrami and (b) Elovich by MgAl/LDH-RSSB at 60 °C.

Table 6 Model parameters and correlation coefficients of pseudo first-order, pseudo second-order, Avrami and Elovich for RBV5R adsorption by MgAl/LDH-RSSB at 30 °C.

Kinetic model	Parameter	Initial RBV5R concentration (mg/l)					
		25	50	100	200	250	300
Pseudo 1st-order	$q_{e,\ exp}$ (mg/g)	14.53	22.16	28.07	35.18	42.38	52.41
	$q_{e,\ cal}$ (mg/g)	14.42	22.17	27.98	35.26	42.40	52.63
	k_1 (min^{-1})	0.7015	0.5427	0.5130	0.4705	0.4212	0.4598
	R_2	0.9929	0.9966	0.9952	0.9933	0.9967	0.9980
Pseudo 2nd-order	$q_{e,\ cal}$ (mg/g)	15.55	24.33	30.82	38.88	47.03	58.07
	k_2 (g/(mg.min))	0.0625	0.0279	0.0205	0.0149	0.0108	0.0097
	R_2	0.9871	0.9767	0.9783	0.9785	0.9859	0.9822
Avrami	$q_{e,\ cal}$ (mg/g)	14.58	21.96	27.70	35.14	42.43	52.45
	k_A (1/s)	0.7095	0.5276	0.4981	0.4635	0.4225	0.4516
	n_A	0.8568	1.1371	1.1358	1.0456	0.9927	1.0509
	R_2	0.9967	0.9987	0.9971	0.9936	0.9968	0.9983
Elovich	α (mg/(g.min)	7.4547	1.6712	1.1189	0.7759	0.4943	0.4862
	β (g/mg)	0.3937	0.2190	0.1691	0.1322	0.1056	0.0877
	R^2	0.9341	0.9199	0.9278	0.9366	0.9527	0.9396

Table 7 Model parameters and correlation coefficients of pseudo first-order, pseudo second-order, Avrami and Elovich for RBV5R adsorption by MgAl/LDH-RSSB at 45 °C.

Kinetic model	Parameter	Initial RBV5R concentration (mg/l)					
		25	50	100	200	250	300
Pseudo 1st-order	$q_{e,\ exp}$ (mg/g)	20.78	32.95	49.88	65.89	76.90	85.99
	$q_{e,\ cal}$ (mg/g)	20.27	32.14	48.93	64.43	75.63	84.56
	k_1 (min^{-1})	0.6792	0.5193	0.4471	0.5327	0.5286	0.5844
	R_2	0.9904	0.9739	0.9920	0.9904	0.9912	0.9909
Pseudo 2nd-order	$q_{e,\ cal}$ (mg/g)	22.03	35.05	54.04	70.58	82.70	92.11
	k_2 (g/(mg.min))	0.0412	0.0196	0.0103	0.0097	0.0083	0.0083
	R_2	0.9956	0.9900	0.9987	0.9965	0.9944	0.9927
Avrami	$q_{e,\ cal}$ (mg/g)	20.64	33.21	49.94	65.76	76.97	85.98
	k_A (1/s)	0.6777	0.5562	0.4744	0.5518	0.5507	0.6002
	n_A	0.8251	0.6898	0.8033	0.8016	0.8129	0.8210
	R_2	0.9957	0.9955	0.9993	0.9975	0.9976	0.9967
Elovich	α (mg/(g.min)	3.8921	1.5094	0.5380	0.6583	0.5760	0.6841
	β (g/mg)	0.2659	0.1589	0.0948	0.0772	0.0662	0.0616
	R^2	0.9511	0.9791	0.9793	0.9692	0.9658	0.9577

$-Ea/R$ slope, which is based on the plot of ln K_2 versus $1/T$ (Figure not shown).

The thermodynamic parameters values of $\Delta H°$ (standard enthalpy), $\Delta G°$ (standard free energy), $\Delta S°$ (standard entropy) and E_a (activation energy) are shown in Table 12. Based on Table 12, it can be observed that the $\Delta H°$ (standard enthalpy) shows positive value. This indicates that the RBV5R adsorption onto the MgAl/LDH-RSSB was endothermic (Bello et al., 2012). The association with endothermic process is highly related to the increased in the rate of diffusion among the RBV5R molecules with the MgAl/LDH-RSSB internal and external boundary pores as the adsorption temperature increases (Wang and Zhu, 2007). Besides, the positive value of $\Delta S°$ (standard entropy) suggest the increase in randomness at solid/solution interface during the RBV5R adsorption process. This signifies that the RBV5R adsorption onto MgAl/LDH-RSSB is associated with mechanism through formation of multi-interactions such as hydrogen bonding, electrostatic attraction, anion exchange and metal complexation) occurred between the RBV5R dye and MgAl/LDH-RSSB (Zubair et al., 2021). The overall changes in the $\Delta G°$ (free energy) at different temperature (303 K − 333 K) is negative. This indicates that the RBV5R adsorption process was spontaneous. Also, $\Delta G°$ were comparatively low (< 20 kJ/mol), suggesting that physisorption is the governed mechanism (Inglezakis, 2007). The E_a (activation energy) value is 25.82 kJ/mol, which was found to be lower than 40 kJ/mol. This indicates that the rate limiting step for RBV5R adsorption on MgAl/LDH-RSSB is mainly controlled by the physical adsorption process (Bello et al., 2012).

6. Insight the mechanism of MgAl/LDH-RSSB for RBV5R removal

In this research study, the adsorption mechanism of MgAl/LDH-RSSB adsorbent towards RBV5R anionic dye was studied in detailed as shown in Scheme 1. At first, the mixed metal

Table 8 Model parameters and correlation coefficients of pseudo first-order, pseudo second-order, Avrami and Elovich for RBV5R adsorption by MgAl/LDH-RSSB at 60 °C.

Kinetic model	Parameter	Initial RBV5R concentration (mg/l)					
		25	50	100	200	250	300
Pseudo 1st-order	$q_{e,\ exp}$ (mg/g)	23.75	41.17	68.99	92.37	112.41	125.88
	q_e, *cal* (mg/g)	23.54	41.28	69.48	91.81	110.70	121.92
	k_1 (min^{-1})	0.4835	0.3372	0.2779	0.3811	0.4356	0.5810
	R_2	0.9929	0.9951	0.9952	0.9881	0.9911	0.9780
Pseudo 2nd-order	q_e, *cal* (mg/g)	25.80	46.56	80.33	102.35	122.11	132.72
	k_2 (g/(mg.min))	0.0240	0.0084	0.0037	0.0045	0.0045	0.0058
	R_2	0.9934	0.9882	0.9871	0.9863	0.9940	0.9977
Avrami	q_e, *cal* (mg/g)	23.87	41.41	69.36	92.83	112.53	126.31
	k_A (1/s)	0.5091	0.3470	0.2724	0.4072	0.4665	0.5992
	n_A	0.8366	0.9526	1.0276	0.8626	0.8163	0.7057
	R_2	0.9981	0.9955	0.9953	0.9913	0.9975	0.9979
Elovich	α (mg/(g.min)	1.4689	0.2961	0.0993	0.1966	0.2371	0.4743
	β (g/mg)	0.2060	0.0995	0.0532	0.0478	0.0421	0.0426
	R^2	0.9658	0.9682	0.9709	0.9679	0.9741	0.9790

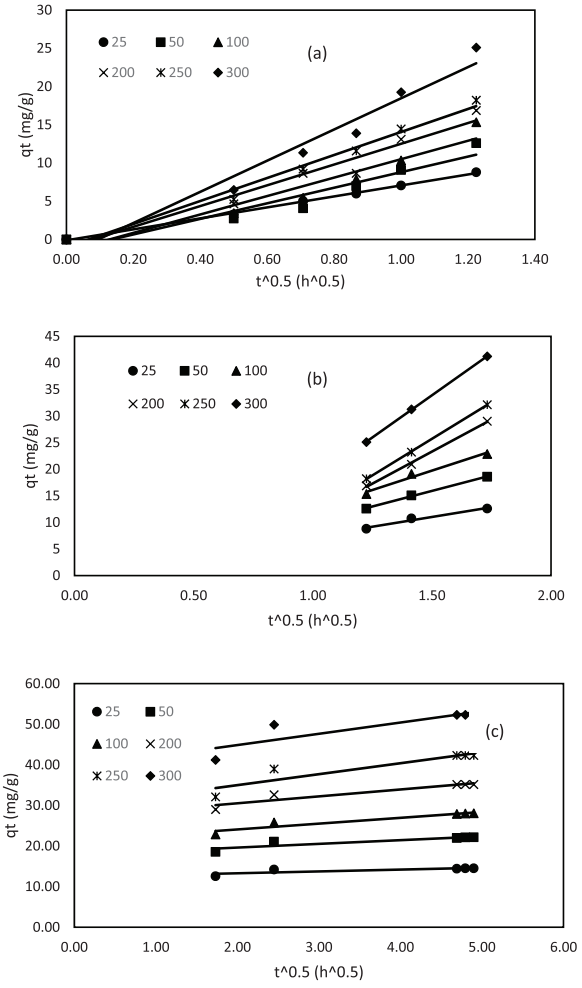

Fig. 17 Intraparticle diffusion plot of MgAl/LDH-RSSB at 30 °C with (a) region from 0 to 1.22 (t^0.5); (b) region from 1.22 to 1.73 (t^0.5); (c) region from 1.73 to 4.90 (t^0.5).

precursors (magnesium nitrate hexahydrate and aluminium nitrate nonahydrate) are synthesized through direct co-precipitation method for 30 min at 60 °C in aqueous solution until complete dissolution was achieved. Subsequently, after the reaction, the mixed metal salts were highly dispersed onto the surfaces of RSSB. Scheme 1 represents the schematic diagram of the synthesis of MgAl/LDH supported on the RSSB.

As seen from Scheme 1, introduction of MgAl-LDH on the RSSB surfaces resulted in the formation of OH– and H_2O functional group. As confirmed by the FTIR, presence of hydroxyl group appeared mainly due to the presence of water molecules found in the middle layer of the adsorbent and might be due to the water molecules that is being physically adsorbed. This suggest that the OH– groups found on the outer layer of the MgAl/LDH-RSSB are the main contributor for the removal of RBV5R anionic dye through chemical interaction and electrostatic attraction (Zubair et al., 2021).

To enhance the performance of LDH, bi (Mg^{2+}) and tri (Al^{3+}) metals were incorporated onto the RSSB as a carbon-based support material. Presence of carbonated group CO_3^{2-} as verified from the FTIR analysis indicates possible involvement of interlayer CO_3^{2-} anions exchange and mixed metal oxides (Al-O and Mg-O) complexation mechanism with RBV5R anions. Overall, the adsorption mechanism of MgAl/LDH-RSSB towards RBV5R was highly associated with multiple reaction processes including chemical complexation, physical adsorption, anionic exchange, electrostatic interaction, and hydrogen bonding (Zubair et al., 2021); (Chakraborty and Acharya, 2018).

7. Comparison study of MgAl/LDH-RSSB with other reported adsorbents

In this study, the adsorption performance of RBV5R onto MgAl/LDH-RSSB was relatively compared with the previous reported adsorbents. Table 13 shows the RBV5R dye comparison in terms of the optimized adsorption conditions together with the maximum adsorption capacity by various carbon-

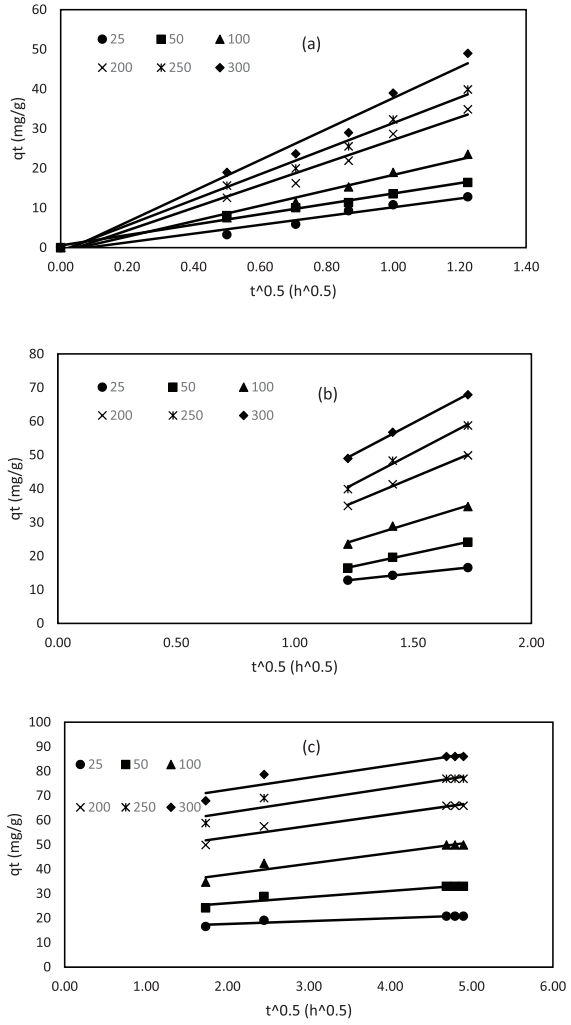

Fig. 18 Intraparticle diffusion plot of MgAl/LDH-RSSB at 45 °C with (a) region from 0 to 1.22 (t^0.5); (b) region from 1.22 to 1.73 (t^0.5); (c) region from 1.73 to 4.90 (t^0.5).

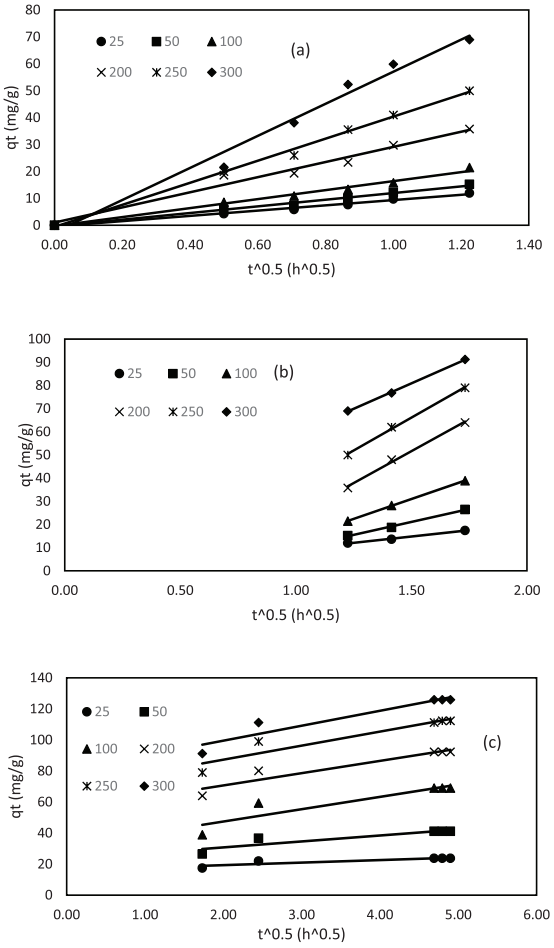

Fig. 19 Intraparticle diffusion plot of MgAl/LDH-RSSB at 60 °C with (a) region from 0 to 1.22 (t^0.5); (b) region from 1.22 to 1.73 (t^0.5); (c) region from 1.73 to 4.90 (t^0.5).

based adsorbent materials. Based on Table 13, the RBV5R adsorption performance on MgAl/LDH-RSSB was better than other reported adsorbents, whereby highest (125.88 mg/g) adsorption capacity was obtained at optimized conditions (300 mg/l concentration, 1440 min and 60 °C temperature). This signifies that the developed MgAl/LDH-RSSB adsorbent had a promising characteristic and was effective for treating colorant wastewater effluent. Overall, the RBV5R adsorption capacity of cocoa pod husk, coconut shells, mango seed, sawdust, coal based activated carbon, gum ghatti alginate hybrid derived titania spheres and calcines eggshell biosorbent displayed lower uptake capacity as compared to the MgAl/LDH-RSSB that is being produced in this research study. Therefore, this suggest that the MgAl/LDH-RSSB has a great advantage to be used an alternative source of adsorbent for remediation of dye effluent.

Table 9 Diffusion mechanism for RBV5R adsorption on MgAl/LDH-RSSB at 30 °C.

Adsorbent	C_o (mg/L)	Intraparticle diffusion model								
		K_{t1}	C_1	R^2	K_{t2}	C_2	R^2	K_{t3}	C_3	R^2
MgAl/LDH-RSSB	25	7.17	0.12	0.9983	7.31	0.05	0.9736	0.46	12.36	0.6843
	50	10.19	1.39	0.919	11.72	1.67	0.9977	0.91	17.79	0.8117
	100	12.06	1.57	0.9221	14.54	2.08	0.9778	1.43	21.23	0.9059
	200	13.58	1.63	0.9524	24.09	12.83	0.9979	1.70	27.13	0.8949
	250	15.06	1.78	0.9821	27.48	15.52	0.9997	2.70	29.60	0.8394
	300	20.41	1.94	0.9587	31.73	17.70	0.9999	2.77	39.35	0.7500

Table 10 Diffusion mechanism for RBV5R adsorption on MgAl/LDH-RSSB at 45 °C.

Adsorbent	C_o (mg/L)	Intraparticle diffusion model								
		K_{t1}	C_1	R^2	K_{t2}	C_2	R^2	K_{t3}	C_3	R^2
MgAl/LDH-RSSB	25	11.08	0.93	0.9612	7.40	0.76	0.9998	1.16	15.28	0.8945
	50	13.09	0.54	0.9895	15.04	1.86	0.9980	2.51	21.02	0.9294
	100	19.44	1.13	0.9854	21.55	2.36	0.9850	4.40	29.07	0.9412
	200	28.52	1.39	0.9809	29.30	3.66	0.9960	4.68	43.61	0.9542
	250	32.24	1.42	0.9902	36.78	4.60	0.9929	5.07	52.87	0.9107
	300	39.05	1.58	0.9795	37.02	5.94	0.9981	5.98	62.41	0.892

Table 11 Diffusion mechanism for RBV5R adsorption on MgAl/LDH-RSSB at 60 °C.

Adsorbent	C_o (mg/L)	Intraparticle diffusion model								
		K_{t1}	C_1	R^2	K_{t2}	C_2	R^2	K_{t3}	C_3	R^2
MgAl/LDH-RSSB	25	9.79	0.40	0.9877	10.84	1.45	0.9945	1.64	16.05	0.8024
	50	12.36	0.43	0.9883	22.35	3.44	0.9952	3.85	23.03	0.8227
	100	16.75	0.58	0.9867	34.28	5.43	0.9998	7.94	31.57	0.8344
	200	28.15	0.64	0.9728	55.05	10.95	0.9955	8.91	54.85	0.9079
	250	41.03	0.69	0.9955	56.78	13.08	0.9979	9.04	69.21	0.8868
	300	59.56	1.86	0.9815	63.99	14.90	0.9993	9.63	80.26	0.9030

Table 12 RBV5R adsorption thermodynamic parameters ($\Delta H°$, $\Delta S°$, E_a, $\Delta G°$) on MgAl/LDH-RSSB.

Adsorbent	$\Delta H°$ (kJ/mol)	$\Delta S°$ (kJ/mol)	E_a (kJ/mol)	$\Delta G°$ (kJ/mol)		
				303 K	318 K	333 K
MgAl/LDH-RSSB	25.82	52.32	29.61	−8.42	−9.14	−9.98

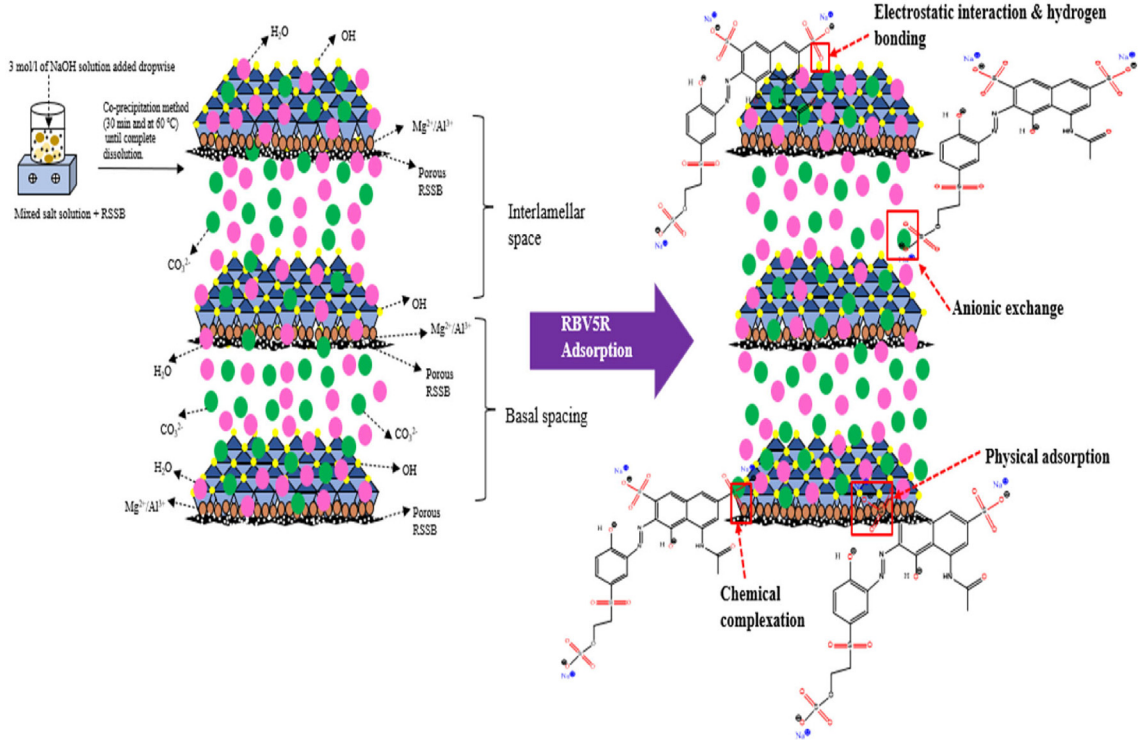

Scheme 1 The adsorption mechanism of MgAl/LDH-RSSB adsorbent towards RBV5R anionic dye removal.

Table 13 Comparison of the RBV5R adsorption performance by MgAl/LDH-RSSB with other reported adsorbents.

Adsorbent	Optimized adsorption conditions			Maximum adsorption capacity (mg/g)	References
	Concentration (mg/l)	Time (min)	Temperature (℃)		
Cocoa pod husk-based activated carbon	100	350	60	76.92	(Bello et al., 2012)
Coconut shells activated carbon	150	1440	30	8.01	(Lai, 2021)
Mango seed activated carbon	150	1440	30	1.26	(Lai, 2021)
Coconut mesocarp	80	1440	30	7.28	(Monteiro et al., 2017)
Sawdust	80	1440	30	0.64	(Monteiro et al., 2017)
Gum ghatti-alginate hybrid derived titania spheres	75	400	25	44.70	(Preeti et al., 2021)
Calcined eggshell biosorbent	100	1440	20	6.93	(Rápó et al., 2019)
Babassu coconut mesocarp	40	30	25	0.857	(Vieira, 2009)
MgAl/LDH-RSSB	**300**	**1440**	**60**	**125.88**	**This study**

8. Conclusion

In this research study, the MgAl/KDH-RSSB was successfully prepared using co-precipitation method. Based on the RBV5R adsorption study, the MgAl/LDH-RSSB adsorbent was favourable, whereby it achieved high adsorption uptake capacity (125.88 mg/g) at initial concentration of 300 ppm, contact time of 1440 min, adsorption temperature of 60 °C and pH 2 compared to the pristine RSSB with only 58.69 mg/g. The adsorption of RBV5R data at different adsorption temperature (30 °C, 45 °C, 60 °C) were best fitted with Freundlich isotherm model, which described the multilayer adsorption that occurs on the heterogeneous MgAl/LDH-RSSB surfaces. The surface area of MgAl/LDH-RSSB (132.40 m^2/g) was found to be larger than pristine RSSB (114.32 m^2/g). The fourier transformed infrared (FTIR) spectroscopy justified the presence of Al-O and Mg-O groups on MgAl/LDH-RSSB surfaces which involve in the enhancement of RBV5R uptake capacity. Besides, the existence of carbonated group CO_3^{2-} indicates possible involvement of interlayer CO_3^{2-} anions exchange and mixed metal oxides (Al-O and Mg-O) complexation mechanism with RBV5R anions. The pseudo first-order kinetic model is the best fitted adsorption kinetic data for 30 °C, 45 °C and 60 °C temperature, whereby the R^2 value was > 0.99 and smaller deviation (< 1%) was observed between the experimental ($q_{e,\ exp}$) and calculated ($q_{e,\ cal}$) values. The thermodynamic study suggested that the adsorption of RBV5R by MgAl/LDH-RSSB was governed by physisorption and endothermic in nature. Overall, the adsorption mechanism of MgAl/LDH-RSSB towards RBV5R anionic dye removal was highly associated with multiple reaction processes including chemical complexation, physical adsorption, anionic exchange, electrostatic interaction, and hydrogen bonding.

Declaration of Competing Interest

The authors declare that they have no known competing financial interests or personal relationships that could have appeared to influence the work reported in this paper.

Acknowledgement

This research is supported by Ministry of Higher Education Malaysia under the Fundamental Research Grant Scheme (project code: FRGS/1/2021/TKO/USM01/3) and post-doctoral award from Universiti Sains Malaysia.

Appendix A. Supplementary material

Supplementary data to this article can be found online at https://doi.org/10.1016/j.arabjc.2023.104643.

References

Abdellaoui, K., Pavlovic, I., Bouhent, M., Benhamou, A., Barriga, C., 2017. A comparative study of the amaranth azo dye adsorption/desorption from aqueous solutions by layered double hydroxides. Appl. Clay Sci. 143, 142–150. https://doi.org/10.1016/j.clay.2017.03.019.

Alberti, G., Amendola, V., Pesavento, M., Biesuz, R., 2012. Beyond the synthesis of novel solid phases: review on modelling of sorption phenomena. Coord. Chem. Rev. 256, 28–45. https://doi.org/10.1016/j.ccr.2011.08.022.

Al-Momani, F., Tourand, E., Degorce-Dumas, J.R., Roussy, J., Thomas, O., 2002. Biodegradability enhancement of textiles dyes and textile wastewater by VUV photolysis. J. Phtochem. Photobiol. A Chem. 153, 191–197.

Amin, M.T., Alazba, A.A., Shafiq, M., 2020. LDH of NiZnFe and its composites with carbon nanotubes and data-palm biochar with efficient adsorption capacity for RB5 dye from aqueous solutions: Isotherm, kinetic, and thermodynamics studies. Curr. Appl. Phys. https://doi.org/10.1016/j.cap.2020.07.005.

Anthonysamy, S.I., Lahijani, P., Mohammadi, M., Mohamed, A.R., 2020. Low temperature adsorption of nitric oxide on cerium impregnated biomass-derived biochar. Korean J. Chem. Eng. 37, 130–140.

Ayed, L., Mahdhi, A., Cheref, A., Bakhrouf, A., 2011. Decolorization and degradation of azo dye Methyl Red by an isolated Sphingomonas paucimobilis: biotoxicity and metabolites characterization. Desalination 274 (1–3), 272–277. https://doi.org/10.1016/j.desal.2011.02.024.

Baharum, N.A., Nasir, H.M., Ishak, M.Y., Isa, N.M., Hassan, M.A., Aris, A.Z., 2020. Highly efficient removal of diazinon pesticide from aqueous solutions by using coconut shell-modified biochar. Arab. J. Chem. 13, 6106–6121. https://doi.org/10.1016/j.arabjc.2020.05.011.

Ballarin, B. et al, 2012. Synthesis route to supported gold nanoparticle layered double hydroxides as efficient catalysts in the electrooxidation of methanol. Langmuir 28, 15065–15074.

Bello, O.S., Ahmad, M.A., 2011. Removal of Remazol Brilliant Violet-5R dye using periwinkle shells. Chem. Ecol. 27, 481–492. https://doi.org/10.1080/02757540.2011.600696.

Bello, O.S., Siang, T.T., Ahmad, M.A., 2012. Adsorption of Remazol Brilliant Violet-5R reactive dye from aqueous solution by cocoa pod husk-based activated carbon: kinetic, equilibrium and thermodynamic studies. Asia-Pacific J. Chem. Eng. 7, 378–388. https://doi.org/10.1002/apj.

Bharali, D., Deka, R.C., 2017. Adsorptive removal of congo red from aqueous solution by sonochemically synthesized NiAl layered double hydroxide. J. Environ. Chem. Eng. 5, 2056–2067. https://doi.org/10.1016/j.jece.2017.04.012.

Bharali, D., Deka, R.C., 2017. Adsorptive removal of congo red from aqueous solution by sonochemically synthesized NiAl layered double hydroxide. J. Environ. Chem. Eng. 5 (2), 2056–2067. https://doi.org/10.1016/j.jece.2017.04.012.

Borhan, A., Yusuf, S., 2020. Activation of rubber-seed shell waste by malic acid as potential CO2 removal: isotherm and kinetics studies. Materials (Basel) 13, 1–20. https://doi.org/10.3390/ma13214970.

A. Chakraborty and H. Acharya, "Facile Synthesis of MgAl-Layered Double Hydroxide Supported Metal Organic Framework Nanocomposite for Adsorptive Removal of Methyl Orange Dye," *Colloids Interface Sci. Commun.*, vol. 24, no. December 2017, pp. 35–39, 2018, doi: 10.1016/j.colcom.2018.03.005

Chen, J., Cao, F., Chen, S., Ni, M., Gao, X., Cen, K., 2014. Adsorption kinetics of NO on ordered mesoporous carbon (OMC) and cerium-containing OMC (Ce-OMC). Appl. Surf. Sci. 317, 26–34. https://doi.org/10.1016/j.apsusc.2014.08.067.

Chen, W.F., Zhang, W.M., Meng, J., 2013. Advances and prospects in research of biochar utilization in agriculture. Sci. Agric. Sin. 46, 3324–3333.

Chong, M.N., Jin, B., Chow, C.W.K., Saint, C., 2010. Recent developments in photocatalytic water treatment technology: A review. Water Res. 44, 2997–3027. https://doi.org/10.1016/j.watres.2010.02.039.

Dai, W. et al, 2021. Characteristics and quantification of mechanisms of Cd2+ adsorption by biochars derived from three different plant-based biomass. Arab. J. Chem. 14,. https://doi.org/10.1016/j.arabjc.2021.103119 103119.

Demirbas, E., Nas, M.Z., 2009. Batch kinetic and equilibrium studies of adsorption of Reactive Blue 21 by fly ash and sepiolite. Desalination 243, 8–21. https://doi.org/10.1016/j.desal.2008.04.011.

Deng, L., Zeng, H., Shi, Z., Zhang, W., Luo, J., 2018. Sodium dodecyl sulfate intercalated and acrylamide anchored layered double hydroxides: a multifunctional adsorbent for highly efficient removal of Congo red. J. Colloid Interface Sci. 521, 172–182. https://doi.org/10.1016/j.jcis.2018.03.040.

Djebbi, M.A. et al, 2016. Preparation and optimization of a drug delivery system based on berberine chloride-immobilized MgAl hydrotalcite. Int. J. Pharm. 506, 438–448. https://doi.org/10.1016/j.ijpharm.2016.04.048.

Du, H. et al, 2022. Performance and mechanisms of NaOH and ball-milling co-modified biochar for enhanced the removal of Cd2+ in synthetic water: a combined experimental and DFT study. Arab. J. Chem. 15,. https://doi.org/10.1016/j.arabjc.2022.103817 103817.

El Hamdouni, Y. et al, 2022. Biomass valorization of walnut shell into biochar as a resource for electrochemical simultaneous detection of heavy metal ions in water and soil samples : preparation, characterization, and applications. Arab. J. Chem. https://doi.org/10.1016/j.arabjc.2022.104252 104252.

Fonts, I., Azuara, M., Gea, G., Murillo, M.B., 2009. Study of the pyrolysis liquids obtained from different sewage sludge. J. Anal. Appl. Pyrolysis 85, 184–191.

Freundlich, H.M.F., 1906. Over the adsorption in solution. J. Phys. Chem. 57, 1100–1107.

Gokulan, R., Avinash, A., Prabhu, G.G., Jegan, J., 2019. Remediation of remazol dyes by biochar derived from Caulerpa scalpelliformis - an eco-friendly approach. J. Environ. Chem. Eng. 7, (5). https://doi.org/10.1016/j.jece.2019.103297 103297.

Gu, Z., Atherton, J.J., Xu, Z.P., 2015. Hierarchical layered double hydroxide nanocomoposites: structure, synthesis and applications. Chem. Commun. 51, 3024–3036.

J. Guarín Romero, J. Moreno-Piraján, and L. Giraldo Gutierrez, "Kinetic and Equilibrium Study of the Adsorption of CO2 in Ultramicropores of Resorcinol-Formaldehyde Aerogels Obtained in Acidic and Basic Medium," *C*, vol. 4, p. 52, 2018, doi: 10.3390/c4040052

Hameed, B.H., Ahmad, A.L., Latiff, K.N.A., 2007. Adsorption of basic dye (methylene blue) onto activated carbon prepared from rattan sawdust. Dye. Pigment 75, 143–149.

B. H. Hameed and a a Ahmad, "Batch adsorption of methylene blue from aqueous solution by garlic peel, an agricultural waste biomass.," *J. Hazard. Mater.*, vol. 164, pp. 870–5, May 2009, doi: 10.1016/j.jhazmat.2008.08.084

Hanafi, M.F., Sapawe, N., 2020. Effect of initial concentration on the photocatalytic degradation of remazol brilliant blue dye using nickel catalyst. Mater. Today Proc. 31, 318–320.

F. Helfferich, *Ion-exchange*. 1962.

H. Hoang Phan Quang *et al.*, "Nitrate removal from aqueous solution using watermelon rind derived biochar-supported ZrO2 nanomaterial: Synthesis, characterization, and mechanism," *Arab. J. Chem.*, vol. 15, p. 104106, 2022, doi: 10.1016/j.arabjc.2022.104106

Holkar, C.R., Jadhav, A.J., Pinjari, D.V., Mahamuni, N.M., Pandit, A.B., 2016. A critical review on textile wastewater treatments: possible approaches. J. Environ. Manage. 182, 351–366. https://doi.org/10.1016/j.jenvman.2016.07.090.

Hou, Y., Yan, S., Huang, G., Yang, Q., Huang, S., Cai, J., 2020. Fabrication of N-doped carbons from waste bamboo shoot shell with high removal efficiency of organic dyes from water. Bioresour. Technol. 303, 122939.

Inglezakis, V.J., 2007. Solubility-normalized Dubinin-Astakhov adsorption isotherm for ion-exchange systems. Micropor. Mesopor. Mater. 103, 72–81. https://doi.org/10.1016/j.micromeso.2007.01.039.

Inyang, M.I. et al, 2016. A review of biochar as a low-cost adsorbent for aqueous heavy metal removal. Crit. Rev. Environ. Sci. Technol. 46, 406–433. https://doi.org/10.1080/10643389.2015.1096880.

Juang, R.-S., Chen, M.-L., 1997. Application of the Elovich equation to the kinetics of metal sorption with solvent-impregnated resins. Ind. Eng. Chem. Res. 36, 813–820.

Kaghazchi, T., Soleimani, M., 2006. Effect of raw materials on properties of activated carbon. Chem. Eng. Technol. 29, 1247–1251.

Kaur, S., Rani, S., Mahajan, R.K., Asif, M., Gupta, V.K., 2015. Synthesis and adsorption properties of mesoporous material for the removal of dye safranin: Kinetics, equilibrium, and thermodynamics. J. Ind. Eng. Chem. 22, 19–27. https://doi.org/10.1016/j.jiec.2014.06.019.

Khare, P., Dilshad, U., Rout, P.K., Yadav, V., Jain, S., 2017. Plant refuses driven biochar: application as metal adsorbent from acidic solutions. Arab. J. Chem. 10, S3054–S3063. https://doi.org/10.1016/j.arabjc.2013.11.047.

Khasri, A., Jamir, M.R.M., Ahmad, A.A., Ahmad, M.A., 2021. Adsorption of remazol brilliant violet 5r dye from aqueous solution onto melunak and rubberwood sawdust based activated carbon: interaction mechanism, isotherm, kinetic and thermodynamic properties. Desalin. Water Treat. 216, 401–411. https://doi.org/10.5004/dwt.2021.26852.

J. Y. Kim, S. Oh, and Y. K. Park, "Overview of biochar production from preservative-treated wood with detailed analysis of biochar characteristics, heavy metals behaviors, and their ecotoxicity," *J. Hazard. Mater.*, vol. 384, no. September 2019, p. 121356, 2020, doi: 10.1016/j.jhazmat.2019.121356.

Kim, T.H., Park, C., Yang, J., Kim, S., 2004. Comparison of disperse and reactive dye removals by chemical coagulation and Fenton oxidation. J. Hazard. Mater. 112, 95–103. https://doi.org/10.1016/j.jhazmat.2004.04.008.

Kudahi, S.N., Noorpoor, A.R., Mahmoodi, N.M., 2017. Determination and analysis of CO2 capture kinetics and mechanisms on the novel graphene-based adsorbents. J. CO2 Util. 21, 17–29. https://doi.org/10.1016/j.jcou.2017.06.010.

Kumar, A., Jena, H.M., 2016. Removal of methylene blue and phenol onto prepared activated carbon from Fox nutshell by chemical activation in batch and fixed-bed column. J. Clean. Prod. 137, 1246–1259. https://doi.org/10.1016/j.jclepro.2016.07.177.

Kuo, Y.-M. et al, 2015. Layered double hydroxide nanpoparticles to enhance organ-specific targeting and the anti-proliferative effect of cisplatin. J. Mater. Chem. B 3, 3447–3458.

Lahijani, P., Mohammadi, M., Mohamed, A.R., 2018. Metal-incorporated biochar as a potential adsorbent for high capacity CO2 capture at ambient condition. J. CO2 Util. 26, 281–293.

Lahijani, P., Mohammadi, M., Mohamed, A.R., 2019. Catalytic CO 2 gasification of rubber seed shell-derived hydrochar: reactivity and kinetic studies. Environ. Sci. Pollut. Res. 26, 11767–11780. https://doi.org/10.1007/s11356-019-04613-4.

Lai, H.J., 2021. Adsorption of Remazol Brilliant Violet 5R (RBV-5R) and Remazol Brilliant Blue R (RBBR) from aqueous solution by using agriculture waste. Trop. Aquat. Soil Pollut. 1 (1), 11–23. https://doi.org/10.53623/tasp.v1i1.10.

S. S. Lam *et al*., "Engineering pyrolysis biochar via single-step microwave steam activation for hazardous landfill leachate treatment," *J. Hazard. Mater*., vol. 390, no. June 2019, p. 121649, 2020, doi: 10.1016/j.jhazmat.2019.121649

Langmuir, I., 1916. The constitution and fundamental properties of solids and liquids. part I. solids. J. Am. Chem. Soc. 38, 2221–2295.

Langmuir, I., 1918. The adsorption of gases on plane surfaces of glass, mica and platinum. J. Am. Chem. Soc. 40, 1361–1403.

Law, X.N. et al, 2022. Microalgal-based biochar in wastewater remediation: its synthesis, characterization and applications. Environ. Res. 204, (PA). https://doi.org/10.1016/j.envres.2021.111966 111966.

Lehmann, J., 2007. A handful of carbon. Nature 447, 143–144.

Li, R. et al, Jul. 2016. Enhancing phosphate adsorption by Mg/Al layered double hydroxide functionalized biochar with different Mg/Al ratios. Sci. Total Environ. 559, 121–129. https://doi.org/10.1016/j.scitotenv.2016.03.151.

Li, X. et al, 2017. Adsorption of reactive yellow X-RG and reactive brilliant red X-3B onto cucurbit[8]uril and cucurbit[6]uril: effect factors, adsorption behavior and mechanism study. J. Colloid Interace Sci. 498, 31–46.

Li, F., Li, G., Zhang, X., 2014. Mechanism of enhanced removal of quinonic intermediates during electrochemical oxidation of orange II under ultraviolet irradiation. J. Environ. Sci. (China) 26, 708–715. https://doi.org/10.1016/S1001-0742(13)60435-0.

Liu, L.Y., Pu, M., Yang, L., Li, D.Q., Evans, D.G., He, J., 2007. Experimental and theoretical study on the structure of acid orange 7-pillared layered double hydroxide. Mater. Chem. Phys. 106, 422–427. https://doi.org/10.1016/j.matchemphys.2007.06.022.

Ma, J. et al, 2012. Enhanced adsorptive removal of methyl orange and methylene blue from aqueous solution by alkali-activatted multi-walled carbon nanotubes. ACS Appl. Mater. Interfaces 4, 5749–5760.

Mandal, S., Tichit, D., Lerner, D.A., Marcotte, N., 2009. Azoic dye hosted in layered double hydroxide: physicochemical characterization of the intercalated materials. Langmuir 25, 10980–10986.

Manna, S., Singh, N., Purakayastha, T.J., Berns, A.E., 2020. Effect of deashing on physico-chemical properties of wheat and rice straw biochars and potential sorption of pyrazosulfuron-ethyl. Arab. J. Chem. 13, 1247–1258. https://doi.org/10.1016/j.arabjc.2017.10.005.

McKay, G., Sweeney, G.A., 1980. Principles of dye removal from textile effluent. Water Air Soil Pollut. 4, 3–11.

Meili, L. et al, 2019. MgAl-LDH/Biochar composites for methylene blue removal by adsorption. Appl. Clay Sci. 168, 11–20. https://doi.org/10.1016/j.clay.2018.10.012.

Memon, J. et al, 2014. Synthesis of graphene/Ni-Al layered double hydroxide nanowires and thier application as an electrode material for supercapacitors. J. Mater. Chem. 2, 5060–5067.

Mokhtar, N.M., Lau, W.J., Ismail, A.F., Veerasamy, D., 2015. Membrane distillation technology for treatment of wastewater from rubber industry in Malaysia. Procedia CIRP 26, 792–796. https://doi.org/10.1016/j.procir.2014.07.161.

Monteiro, M.S., de Farias, R.F., Chaves, J.A.P., Santana, S.A., Silva, H.A.S., Bezerra, C.W.B., 2017. Wood (Bagassa guianensis Aubl) and green coconut mesocarp (cocos nucifera) residues as textile dye removers (Remazol Red and Remazol Brilliant Violet). J. Environ. Manage. 204, 23–30. https://doi.org/10.1016/j.jenvman.2017.08.033.

Mustapha Bouhent, M., Derriche, Z., Denoyel, R., Prevot, V., Forano, C., 2011. Thermodynamical and structural insights of orange II adsorption by Mg RAlNO3 layered double hydroxides. J. Solid State Chem. 184, 1016–1024. https://doi.org/10.1016/j.jssc.2011.03.018.

Nadarajah, R.Y., Mohammad, R., Mohamad, M., 2018. Rubber seed shells (Hevea Brasiliensis): an adsorbent used for the removal of Rhodamine B dye. ARPN J. Eng. Appl. Sci. 13 (24), 9311–9317.

Oliveira, G.F.D., Andrade, R.C.D., Trindade, M.A.G., Andrade, H.M.C., Carvalho, C.T.D., 2016. Thermogravimetric and spectroscopic study (TG-DTA/FT-IR) of activated carbon from the renewable biomass source Babassu. Quim. Nova 40, 284–292.

Preeti, S. Banerjee, A. Debnath, and V. Singh, "Gum ghatti-alginate hybrid bead derived titania spheres for deep removal of toxic dye Remazol Brilliant Violet from aqueous solutions," *Environ. Nanotechnology, Monit. Manag*., vol. 15, no. October 2020, p. 100459, 2021, doi: 10.1016/j.enmm.2021.100459

Rahman, M.Z., Edvinsson, T., Kwong, P., 2020. Biochar for electrochemical applications. Curr. Opin. Green Sustain. Chem. 23, 123950.

Rápó, E., Posta, K., Suciu, M., Szép, R., Tonk, S., 2019. Adsorptive removal of Remazol Brilliant Violet-5R dye from aqueous solutions using calcined eggshell as biosorbent. Acta Chim. Slov. 66, 648–658. https://doi.org/10.17344/acsi.2019.5079.

Rashidi, N.A., Yusup, S., Ahmad, M.M., Mohamed, N.M., Hameed, B.H., 2012. Activated carbon from the renewable agricultural residues using single step physical activation: a preliminary analysis. APCBEE Procedia 3, 84–92.

Reshad, A.S., Tiwari, P., Goud, V.V., 2018. Thermo-chemical conversion of waste rubber seed shell to produce fuel and value-added chemicals. J. Energy Inst. 91, 940–950.

Sahoo, M., Singha, S., Parida, K.M., 2011. Amine functionalized layered double hydroxide: a reusable catalyst for aldol condensation. New J. Chem. 35, 2503–2509.

Senthilkumaar, S., Varadarajan, P.R., Porkodi, K., Subbhuraam, C.V., 2005. Adsorption of methylene blue onto jute fiber carbon: kinetics and equilibrium studies. J. Colloid Interface Sci. 284, 78–82. https://doi.org/10.1016/j.jcis.2004.09.027.

Srivatsav, P., Bhargav, B.S., Shanmugasundaram, V., Arun, J., Gopinath, K.P., Bhatnagar, A., 2020. Biochar as an eco-friendly and economical adsorbent for the removal of colorants (Dyes) from aqueous environment: a review. Water (Switzerland) 12, 1–27. https://doi.org/10.3390/w12123561.

Temkin, M.J., Pyzhev, V., 1940. Recent modifications to Langmuir isotherms. Acta Phys.-Chem. Sin. 12, 217–222.

Thangaraj, S., Bankole, P.O., Sadasivam, S.K., 2021. Microbial degradation of azo dyes by textile effluent adapted, Enterobacter hormaechei under microaerophilic condition. Microbiol. Res. 250,. https://doi.org/10.1016/j.micres.2021.126805 126805.

Thitame, P.V., Shukla, S.R., 2016. Adsorptive removal of reactive dyes from aqueous solution using activated carbon synthesized from waste biomass materials. Int. J. Environ. Sci. Technol. 13, 561–570.

Vieira, A.P. et al, 2009. Kinetics and thermodynamics of textile dye adsorption from aqueous solutions using babassu coconut meso-

carp. J. Hazard. Mater. 166 (2–3), 1272–1278. https://doi.org/10.1016/j.jhazmat.2008.12.043.

Wang, X. et al, 2013. Self-assembly of Ni-Fe layered double hydroxide/graphene hybrids for reducing fire hazard in epoxy composites. J. Mater. Chem. A 1, 4383–4390.

Wang, L. et al, 2018. Microwave assisted modification of activated carbons by organic acid ammoniums activation for enhanced adsorption of acid red 18. Powder Technol. 323, 230–237. https://doi.org/10.1016/j.powtec.2017.10.021.

Wang, J. et al, 2022. Remediation of Cd2+ in aqueous systems by alkali-modified (Ca) biochar and quantitative analysis of its mechanism. Arab. J. Chem. 15,. https://doi.org/10.1016/j.arabjc.2022.103750 103750.

Wang, S., Gao, B., Li, Y., Zimmerman, A.R., Cao, X., 2016. Sorption of arsenic onto Ni/Fe layered double hydroxide (LDH)-biochar composites. RSC Adv. 6, 17792–17799.

Wang, S., Zhu, Z.H., 2007. Effects of acidic treatment of activated carbons on dye adsorption. Dye. Pigment 75, 306–314.

Wu, H., Feng, Q., 2017. Fabrication of bimetallic Ag/Fe immobilized on modified biochar for removal of carbon tetrachloride. J. Environ. Sci. (China) 54, 346–357. https://doi.org/10.1016/j.jes.2016.11.017.

Xia, S., Zhang, L., Pan, G., Qian, P., Ni, Z., 2015. Photocatalytic degradaion of methylene blue with a nanocomposite system: synthesis, photocatalysis and degradation pathways. Phys. Chem. Chem. Phys. 17, 5345–5351.

Xie, R., Fan, G., Ma, Q., Yang, L., Li, F., 2014. Facile synthesis and enhanced catalystic performance of graphene-supported Ni nanocatalyst from a layered double hydroxide based caomposite precursor. J. Mater. Chem. 2, 7880–7889.

Xu, Y., Xia, H., Zhang, Q., Jiang, G., Cai, W., Hu, W., 2022. Adsorption of cadmium(II) in wastewater by magnesium oxide modified biochar. Arab. J. Chem. 15,. https://doi.org/10.1016/j.arabjc.2022.104059 104059.

Youn, D.H., Bin Park, Y., Kim, J.Y., Magesh, G., Jang, Y.J., Lee, J. S., 2015. One-pot synthesis of NiFe layered double hydroxide/reduced graphene oxide composite as an efficient electrocatalyst for electrochemical and photoelectrochemical water oxidation. J. Power Sources 294, 437–443. https://doi.org/10.1016/j.jpowsour.2015.06.098.

Yu, B. et al, 2015. Magnetic graphene sponge for the removal of methylene blue. Appl. Surf. Sci. 351, 765–771. https://doi.org/10.1016/j.apsusc.2015.05.185.

Zangeneh, H., Zinatizadeh, A.A.L., Habibi, M., Akia, M., Hasnain Isa, M., 2015. Photocatalytic oxidation of organic dyes and pollutants in wastewater using different modified titanium dioxides: a comparative review. J. Ind. Eng. Chem. 26, 1–36. https://doi.org/10.1016/j.jiec.2014.10.043.

Zhang, X. et al, 2022. Hierarchically porous tobacco midrib-based biochar prepared by a simple dual-templating approach for highly efficient Rhodamine B removal. Arab. J. Chem. 15,. https://doi.org/10.1016/j.arabjc.2022.103904 103904.

Zhang, M., Gao, B., Yao, Y., Inyang, M., 2013. Phosphate removal ability of biochar/MgAl-LDH ultra-fine composites prepared by liquid-phase deposition. Chemosphere 92, 1042–1047.

Zhang, M., Yao, Q., Lu, C., Li, Z., Wang, W., 2014. Layered double hydroxide-carbon dot composite: high performance adosorbent for removal of anionic organic dye. ACS Appl. Mater. Interfaces 6, 20225–20233.

Zhu, Z. et al, 2016. Effect of polymeric matrix on the adsorption of reactive dye by anion-exchange resins. J. Taiwan Inst. Chem. Eng. 62, 98–103. https://doi.org/10.1016/j.jtice.2016.01.017.

Zubair, M., Aziz, H.A., Ahmad, M.A., Ihsanullah, I., Al-Harthi, M. A., 2021. Adsorption and reusability performance of M-Fe (M = Co, Cu, Zn and Ni) layered double hydroxides for the removal of hazardous Eriochrome Black T dye from different water streams. J. Water Process Eng. 42,. https://doi.org/10.1016/j.jwpe.2021.102060 102060.